SUSTAINABLE AND RECOVERABLE WASTE-BASED MAGNETIC NANOCOMPOSITES USED FOR THE REMOVAL OF PHARMACEUTICALS FROM WASTEWATER

Luciana S. Rocha[1,*], Érika M.L. Sousa[1], Diogo Pereira[1], María V. Gil[2], Gonzalo Otero-Irurueta[3], María J. Hortigüela Gallo[3], Marta Otero[4], Valdemar I. Esteves[1], Vânia Calisto[1]

[1] Department of Chemistry and CESAM, University of Aveiro, 3810-193 Aveiro, Portugal

[2] Instituto de Ciencia y Tecnología del Carbono, INCAR-CSIC, Francisco Pintado Fe 26, 33011 Oviedo, Spain

[3] TEMA-NRD, Mechanical Engineering Department, University of Aveiro, 3810-193 Aveiro, Portugal

[4] Department of Environment and Planning and CESAM, University of Aveiro, 3810-193 Aveiro, Portugal

ABSTRACT

This work aimed at producing easily recoverable magnetic iron-oxide functionalized activated carbons (AC) through environmentally and energetically sustainable methods, evaluating their efficacy towards the removal of the pharmaceuticals diclofenac (DCF) and venlafaxine (VEN) from different aqueous matrices (ultrapure water and wastewater treatment plant effluents). Two AC were prepared by chemical activation of a biomassic industrial waste followed by either conventional (CP) or microwave (MW) pyrolysis. Then, magnetic iron oxide nanoparticles were loaded onto the produced AC. Differences related to the production procedure were not especially remarkable, since both the resulting magnetic composites (MAC-CP and MAC-MW) presented well-developed micropore structures with specific surface areas of 644 and 548 m^2 g^{-1} and saturation magnetization of 32.9 and 22.5 emu g^{-1}, respectively, which conferred them a high adsorptive performance and efficient magnetic recovery from

solution. The kinetic data were well described by both pseudo-first and pseudo-second order models. As for the equilibrium data, Langmuir isotherm provided a good fitting, with maximum adsorption capacities ranging between 97±2 and 215±4 µmol g^{-1} for MAC-CP and between 80±2 and 172±3 µmol g^{-1} for MAC-MW. Additionally, in binary (DCF and VEN) solutions and wastewater, adsorption onto both MAC was somewhat inhibited due to competitive effects. MW-assisted regeneration of exhausted MAC was effective, as their adsorptive properties and chemical surface features (according to X-Ray photoelectron spectroscopy) remained unchanged. Overall, the produced waste-based magnetic carbon composites simultaneously combine high adsorptive efficiency, easy retrievability and successful regeneration/reutilization.

1. INTRODUCTION

Pharmaceuticals represent a milestone in scientific development, being responsible for increasing life-expectancy and improving quality of life. However, the wide consumption of pharmaceuticals has led to their widespread occurrence in the environment in both unchanged and metabolized forms, and for that reason, they emerge as increasingly occurring contaminants. The environmental incidence of pharmaceuticals in aquatic systems highlights, on one side, their persistent nature, and on the other, the inefficiency of conventional methods used in water and wastewater treatment for their removal [1–4]. In order to surpass these issues, the Directive 2013/39/EU established the need to monitor some pharmaceuticals and assess their environmental impact on both aquatic environment and human health, while encouraging the development and implementation of complementary and cost-effective methodologies capable of adequately removing these emerging contaminants [5].

Some advanced technologies have been proposed for the uptake of pharmaceuticals and other contaminants from water and wastewater. Adsorption has been regarded as a promising method in the field of water treatment and pollution control due to the simple design and operation mode and no by-product formation [2,4,6]. Adsorption by means of highly porous activated carbon (AC) represents an attractive option for advanced wastewater treatment. Nevertheless, some flaws have been reported regarding the practical application of AC in wastewater treatment plants (WWTP), including: 1) high cost, which is mostly derived from the use of unsustainable materials/methods in their production; 2) difficult after-use separation and regeneration of spent AC for reutilization, particularly for powdered AC, limiting their life-cycle [7–10]. The utilization of waste-based AC produced by environmentally and energetically sustainable processes is a possible solution to overcome high AC prices. Recent studies have shown

that microwave (MW) pyrolysis represents a viable and favourable alternative to conventional pyrolysis [11–13], allowing for the production of adsorbent materials equally efficient towards the removal of pharmaceuticals from water [14–17]. MW irradiation ensures an uniform, fast and selective heating, which leads to short synthesis cycles, high production yields and excellent energy efficiency, and thus, it represents an environmentally friendly technology [12,18,19]. Moreover, the preparation of waste-based AC anchored with ferromagnetic metal oxides (e.g. iron oxides), has been pointed as a suitable solution to avoid the time consuming and inefficient filtration or centrifugation after-use separation stages [7,20,21]. In this way, the depleted magnetic activated carbons (MAC) could be easily and quickly recovered from treated water by applying an external magnetic field and then subjected to regeneration for subsequent reuse.

In view of a sustainable application, the after-use regeneration of MAC is essential and chemical regeneration has been frequently used to restore the adsorption capacity of exhausted MAC [22–25]. However, such regeneration, particularly if using organic solvents, is not an environmentally friendly solution, resulting in the generation of secondary pollution. In order to avoid the use of chemicals, thermal regeneration of MAC by conventional pyrolysis has been carried out with success [22,26]. Alternatively to conventional thermal processes, which typically require temperatures ranging between 700 and 900 ºC and mild oxidizing or inert conditions applied for long periods of time [27,28], MW regeneration has been shown to be advantageous in the regeneration of AC due to its capacity to provide homogeneous and rapid thermal reactions so representing important time, inert gases and energy savings [27–30]. In addition, MW-assisted regeneration avoids the deterioration and preserves the porous structure of the regenerated carbon-based adsorbent materials [29–31]. Although MW heating has been pointed as a

more sustainable option with unique features for AC regeneration [28,32], to the best of the authors' knowledge, only the study by Wang et al. (2014) used MW for the regeneration of MAC after saturation with 2,4,6-TCP and there are no published studies for MAC saturated with pharmaceuticals [33].

Aiming at the assessment of the viability of using waste-based MAC for the sustainable removal of pharmaceuticals from wastewater, this study focused on: (i) the comparison, for the very first time, of the effects of different thermal treatments in the production of sustainable waste-based magnet-responsive iron oxide-functionalized powdered AC; and (ii) the evaluation of their after-use regeneration by MW and subsequent reutilization. An industrial waste from paper industry was used as alternative raw material to non-renewable carbon sources to produce two different waste-based AC, following the optimized procedure reported by Jaria et al. (2019) using conventional pyrolysis (CP) [34] and that proposed by Sousa *et al.* (2021) using MW heating [17]. The resulting materials were then loaded with magnetic iron oxide nanoparticles to obtain MAC-CP and MAC-MW, respectively. These two MAC were compared regarding their physicochemical properties and their adsorptive performance towards the removal of the non-steroidal anti-inflammatory diclofenac (DCF) and the antidepressant venlafaxine (VEN) from ultrapure water and from real WWTP effluents. Since the inclusion of DCF in the first watch list (Decision 2015/495/EU) [35] and, more recently, VEN in the third watch list (Decision 2020/1161/EU) [36], these two pharmaceuticals have received more attention in the context of the European Water Framework Directive (Directive 2000/60/EC, Directive 2013/39/EU), as they are regarded as high-risk substances to be prioritized [5,37]. Thus, the adsorption kinetics and equilibrium of DCF and VEN, together with competitive effects in binary systems and regeneration-reutilization performance, were studied in the present work.

2. MATERIALS AND METHODS

2.1. Chemicals

Potassium hydroxide (KOH, LABCHEM, ≥86 %) was used as activating agent for AC production and in the synthesis of MAC. Diluted hydrochloric acid (HCl, AnalaR NORMAPUR, 37 %) was used to wash the AC produced by conventional and MW-assisted pyrolysis. Ferrous sulphate heptahydrate ($FeSO_4 \cdot 7H_2O$, >99 %) and ferric chloride hexahydrate ($FeCl_3 \cdot 6H_2O$, >99 %) were acquired from Chem-Lab. Buffer solutions of 4.01±0.01, 7.01±0.01 and 10.1±0.01 from Hanna Instruments were used for pH meter calibration. Sodium hydroxide (NaOH, 99.3%, José Manuel Gomes dos Santos) solutions (0.1 and 0.5 mol L^{-1}) were used for pH adjustments. The pharmaceuticals used in the adsorption tests were sodium diclofenac salt ($C_{14}H_{10}Cl_2NNaO_2$, TCI, >98 %) and venlafaxine hydrochloride ($C_{17}H_{28}ClNO_2$, TCI, >98 %). Regarding the pharmaceuticals quantification, the following reagents were used: hexadimethrine bromide (($C_{13}H_{30}Br_2N_2)_n$, Sigma, 95 %) for capillary coating, ethylvanillin ($C_2H_5OC_6H_3(OH)CHO$, Sigma-Aldrich, 99 %) as internal standard, and sodium dodecyl sulfate ($CH_3(CH_2)_{11}OSO_3Na$, PanReac, PA-ACS) and sodium tetraborate decahydrate ($Na_2B_4O_7 \cdot 10H_2O$, Riedel-de-Haën) as separation buffers. All solutions were prepared in ultrapure water (18.2 MΩ cm^{-1}, PURELAB flex 4 system, ELGA VEOLIA).

2.2. Preparation of Activated Carbons

Primary sludge (PS) from a pulp and paper mill, which uses eucalyptus (*Eucalyptus globulus*) wood and employs the kraft elemental chlorine free production process, was used as raw material (PS ultimate and proximate analysis are depicted in Table S1 of SM). Two powdered AC were produced from PS: AC-CP was prepared by conventional pyrolysis and AC-MW was prepared by MW-assisted pyrolysis. The raw

material and experimental setups used to produce AC-CP and AC-MW were the optimized procedures used by Jaria et al (2019) (to produce the material named as AC3) [34] and by Sousa et al. (2021) (to produce the material named as MW800-20-1:5) [17], respectively. Still, PS from this paper mill was proved by Jaria et al. (2017) to have consistent properties, which is essential for the application of optimized procedures for the production of reliable and steady carbon adsorbents [38]. In summary, PS was impregnated with KOH (used as activating agent) under ultrasonic stirring for 1 h and using the following KOH:PS *w/w* ratios: 1:1 for AC-CP and 1:5 for AC-MW. Then, impregnated wastes were dried at room temperature in a laboratory fume hood and pyrolyzed under N_2 atmosphere. The AC-CP was obtained from carbonization by conventional heating in a muffle furnace (Nüve, series MF 106) at 800 ºC for 150 min (heating rate of 10 °C min^{-1}) and using porcelain crucibles [34]. For AC-MW, MW radiation was applied in an industrial MW furnace (Phoenix ™ AirWave CEM, dimensions 46.15 × 65.40 × 49.78 cm (w x d x h)) at 800 °C during 20 min (heating rate of 15 °C min^{-1}) and using quartz crucibles [17]. After carbonization, the resulting materials were first washed with 1.0 M HCl (for ashes removal) and then with distilled water (until neutral pH of the leachate was achieved) followed by overnight drying at 100 ºC. Finally, and aiming to obtain a fine homogenous powder, AC-CP and AC-MW were crushed and sieved to obtain a particle diameter ≤ 180 µm.

2.3. Preparation of Magnetic Activated Carbons

The synthesis of MAC was performed by *in-situ* co-precipitation of magnetic iron oxides onto AC-CP and AC-MW. The reaction was conducted in the presence of a N_2 flux to prevent the formation of non-magnetic forms of iron oxides. Optimal production conditions were selected based on a multivariable optimization method through a

fractional factorial design carried out in a previous study [39]. Briefly, 50 mL of a solution containing both 36.8 mmol L^{-1} $FeSO_4 \cdot 7H_2O$ and 73.1 mmol L^{-1} $FeCl_3 \cdot 6H_2O$ salts (1:2 molar ratio) was prepared in ultrapure water (UW) degassed with N_2, transferred to a glass reactor and heated at 80 ºC. Then, 375 mg of AC-CP or AC-MW (prepared according with the procedure described in section 2.2) (AC: total Fe salts w/w ratio of 1:4) were added to the pre-heated solution and the mixture was stirred at 100 rpm, under oxygen-free conditions (N_2 flux), kept during the whole process. The co-precipitation of iron oxides was accomplished by the dropwise addition of 50 mL of 0.56 mol L^{-1} KOH to attain a pH value of 13.5±0.5. The reaction was carried out for 1 h, maintaining the defined temperature. The MAC obtained were magnetically decanted, the supernatant was discarded, and the materials were thoroughly washed with distilled water until the pH of the washing leachate was neutral. Subsequently, MAC-CP and MAC-MW were dried at 50 ºC, mechanically ground and stored in a sealed container prior to their use. For comparison purposes, bare iron magnetic nanoparticles (Fe-MNP) were prepared via the co-precipitation of Fe^{3+} and Fe^{2+} salts in alkaline medium according with the experimental procedure described above, but with no AC added to the reaction pot.

2.4. Characterization of materials

2.4.1. Specific surface area and pore morphology

The surface area and porosity features of Fe-MNP, AC-CP, AC-MW, MAC-CP and MAC-MW were evaluated by N_2 adsorption isotherms using a Micromeritics Gemini VII 2380 Analyzer system (USA). The materials were first outgassed overnight at 120 °C and then, adsorption and desorption isotherms were conducted at liquid nitrogen temperature (−196 °C). The following set of parameters were determined: specific surface area (S_{BET}), total micropore volume (W_0), total pore volume (V_p) and average pore width (D). To determine S_{BET}, the Brunauer-Emmett-Teller (BET) equation [40] was used, at

relative pressures ranging between 0.01 and 0.1, while W_0 was determined by the Dubinin-Radushkevich equation [41]. V_p was estimated from the amount of N_2 adsorbed at a relative pressure of 0.99 and D was determined by using the following equation $D= 2 \times V_p/S_{BET}$ [42]. The pore size distribution was determined by Non-Local Density Functional Theory (NLDFT) analysis assuming slit pores.

2.4.2. Vibrating sample magnetization

The saturation magnetization (M_s) of MAC-CP and MAC-MW was determined using a vibrating sample magnetometer (VSM EV9). The instrument was first calibrated with a disk of pure nickel and applying a magnetic field of *c.a.*1 Oe and with dispersion on the magnetic moment inferior to 0.5 %. Then, the measurements were performed using an applied magnetic field to a maximum of 22 kOe. The magnetic moment was plotted as a function of the applied magnetic field and M_S was calculated by the ratio between the *plateau* found for the magnetic moment and the mass of material (10 mg). For comparison purposes, VSM analysis was also conducted for Fe-MNP, AC-CP and AC-MW.

2.4.3. Point of zero charge

The point of zero charge (pH_{PZC}) of each material was measured using the pH drift method, which involves the preparation of a set of NaCl 0.1 M aqueous solutions with pH initial values (pH_i) ranging between 2 and 11. These pH values were set with either HCl (0.1 M and 0.01 M) and/or NaOH (0.1 M and 0.01 M). Then, prepared solutions (40 mL) were incubated with 1 mg of each MAC in propylene tubes, and the system was stirred in an overhead shaker for 24 h at 25 °C. Each solution was filtered, and its final pH (pH_f) was measured. By plotting Δ_{pH} (pH_f– pH_i) as a function of pH_i, the values for pH_{PZC} are determined from the pH value corresponding to the *x*-axis interception of the obtained curve.

2.4.4. X-ray photoelectron spectroscopy

The surface chemical composition of the produced materials was evaluated by X-ray photoelectron spectroscopy (XPS). The XPS spectra were acquired in an Ultra High Vacuum (UHV) system with a base pressure of $2x10^{-10}$ mbar. The system is equipped with a hemispherical electron energy analyser (SPECS Phoibos 150), a delay-line detector and a monochromatic AlKα (1486.74 eV) X-ray source. High resolution spectra were recorded at normal emission take-off angle and with a pass-energy of 20 eV, which provides an overall instrumental peak broadening of 0.5 eV.

2.5. Characterization of wastewater treatment plant effluent

The effluent (EF) was collected from the outlet of a WWTP located in the urban area of Aveiro, Portugal (40°36'17.2"N 8°42'34.0"W), which receives an average wastewater flow of 39,278 m^3 per day and performs primary and biological treatments. After collection, the EF was autoclaved at 90 ºC for a period of 45 minutes to inactivate microorganisms and stop biodegradation processes in the matrix. This step was followed by vacuum filtration using a 0.45μm Supor-450 cellulose membrane disc filter, in order to remove suspended particulate matter. Finally, the filtered EF was stored at 4 °C in the absence of light until its use (within a maximum of three weeks). The EF was characterized in terms of pH (Hanna Instruments, HI2020-02 pH meter), conductivity (WTW meter) and dissolved organic carbon (DOC) (Shimadzu, TOC-VCPH liquid sample module SSM-5000A, Japan). The values determined were as follows: pH= 8.4, conductivity = 2.5 mS cm^{-1} and DOC= 17.1±0.7 mg L^{-1}.

2.6. Adsorption studies

Batch adsorption experiments were carried out to evaluate the efficiency of MAC-CP and MAC-MW in the removal of DCF and VEN from aqueous media. The physico-chemical properties and chemical structures of both pharmaceuticals are presented in Table S2 of Supplementary Material (SM). Individual and binary solutions of DCF and VEN with an initial concentration (C_i) of 14 μmol L^{-1} of each pharmaceutical were prepared in both ultrapure water (UW, pH adjusted to 7.5±0.1) and WWTP effluent (EF, pH 8.4). The experiments were performed in 50 mL polypropylene tubes, in which a selected amount of MAC-CP or MAC-MW was placed in contact with 40 mL of each pharmaceutical solution and stirred overnight in an overhead shaker (Heidolph, Reax 2) at 80 rpm under controlled temperature (25.0±0.1 °C). Then, solution aliquots were withdrawn from stirred tubes at pre-defined times, filtered through 0.22 μm PVDF filters (Whatman) and analysed for the remaining pharmaceutical concentration (C_f). The analytic quantification was performed by MEKC, according to the procedure described in section S1 in SM. All the sorption experiments were performed in triplicate and in parallel with blank controls with the same C_i (14 μmol L^{-1} of either DCF or VEN) but no MAC. At the pre-defined times, aliquots were withdrawn from controls and analysed for the concentration of the corresponding pharmaceutical (C_c), which was used as reference for the calculation of adsorption percentages (A, %) for each pharmaceutical, using equation (1):

$$A = \frac{C_c - C_f}{C_c} \times 100 \tag{1}$$

2.6.1. Kinetic adsorption studies

The adsorption kinetics of single DCF and VEN solutions (C_i of 14 μmol L^{-1}) with each MAC were performed in both UW and EF. A known amount of MAC-CP and MAC-MW was added to each test tube, followed by agitation for specific time intervals (5, 10,

15, 30, 60, 120 and 240 min). Regarding the adsorption experiments performed in UW, a dose (mass of adsorbent per volume of adsorbate solution) of 35 mg L^{-1} was used. As for those conducted in EF, due to matrix effects, a higher adsorbent dose was used, and the value selected for each system was 85 mg L^{-1}. After the corresponding agitation time interval, aliquots were withdrawn from polypropylene tubes, filtered and analysed by MEKC (procedure described in section S1 in SM). The amount of pharmaceutical adsorbed at each time (q_t, µmol g^{-1}) was determined by Eq. (2):

$$q_t = \frac{(C_c - C_t)V}{m_{MAC}} \qquad (2)$$

where C_t (µmol L^{-1}) is the pharmaceutical concentration in the aqueous phase at time t (min), V (mL) is the volume of solution and m_{MAC} (mg) is the mass of each MAC used.

2.6.2. Equilibrium adsorption studies

The equilibrium data of MAC-CP and MAC-MW for individual solutions containing DCF and VEN were obtained, maintaining the initial concentration of each pharmaceutical (C_i of 14 µmol L^{-1}) and varying the adsorbent dose. Regarding the equilibrium experiments performed in UW, the dose of MAC ranged between 10 mg L^{-1} and 100 mg L^{-1}, except for the DCF:MAC-MW system, for which up to 200 mg L^{-1} of material were used. For the experiments conducted in EF, the dose of MAC varied between 35 mg L^{-1} and 200 mg L^{-1}. Polypropylene tubes were agitated during 180 min to ensure equilibrium (as inferred from kinetic results), followed by aliquots withdrawal, filtration and analysis by MEKC (as described in section S1 in SM). The loading of DCF and VEN on the corresponding MAC at equilibrium (q_e, µmol g^{-1}) was determined according to Eq. (3):

$$q_e = \frac{(C_c - C_f)V}{m_{MAC}} \qquad (3)$$

2.6.3. Competitive adsorption studies

Competitive adsorption experiments were conducted using binary solutions containing DCF and VEN (C_i of 14 μmol L^{-1}), according with the procedure described in section 2.6. The binary solutions were prepared in both UW and EF, adding 35 mg L^{-1} or 85 mg L^{-1} of the material under study, respectively. Subsequently, binary solutions were subjected to agitation for a time interval of 180 min.

2.6.4. Regeneration and reutilization

The regeneration of MAC-CP and MAC-MW was evaluated after one adsorption cycle with 14 μmol L^{-1} DCF solution prepared in UW and agitation during 180 min. The MAC-CP and MAC-MW affording removal efficiencies above 85 %, were collected by magnetic decantation and dried in the oven at 40 °C for 48 h. After that, the regeneration was conducted under an inert atmosphere in a Phoenix ™ AirWave CEM industrial MW furnace. Considering the thermogravimetric profiles of both pharmaceuticals (see Figure S1 in SM), a MW temperature of 400 ºC (heating rate of 15 °C min^{-1}) was applied and a residence time of 20 min was used.

The feasibility of the above-described regeneration was evaluated by using the regenerated MAC-CP and MAC-MW in a second adsorption cycle. Thus, individual and binary solutions containing C_i of 14 μmol L^{-1} of DCF and VEN prepared in UW were put under agitation together with 35 mg L^{-1} of each regenerated MAC for a time interval of 180 min. Furthermore, the surface chemical composition of the regenerated MAC-CP and MAC-MW was analysed by XPS, as described in section 2.4.4., and compared with virgin materials.

2.6.5. Kinetic and equilibrium models

i) Kinetic models

The kinetic profiles of DCF and VEN uptakes by MAC-CP and MAC-MW were modelled by pseudo-first-order (P1O) [43] and pseudo-second-order (P2O) [44] kinetic reaction-based models, which are respectively expressed by Eqs. (4) and (5):

$$q_t = q_e[1 - exp(-k_1 t)] \tag{4}$$

$$q_t = \frac{k_2 q_e^2 t}{1 + k_2 q_e t} \tag{5}$$

in which k_1 (min^{-1}) is the P1O rate constant and k_2 ($\text{g } \mu\text{mol}^{-1} \text{min}^{-1}$) the P2O rate constant.

ii) Equilibrium models

The equilibrium data were modelled by the Langmuir [45] and Freundlich [46] isotherms, mathematically represented by Eqs. (6) and (7), respectively:

$$q_e = \frac{q_m K_L C_e}{1 + K_L C_e} \tag{6}$$

$$q_e = K_F C_e^{1/n} \tag{7}$$

where C_e ($\mu\text{mol L}^{-1}$) is the concentration of each pharmaceutical at equilibrium in the solution, q_{mL} ($\mu\text{mol g}^{-1}$) is the Langmuir sorption capacity corresponding to complete monolayer coverage, K_L ($\text{L } \mu\text{mol}^{-1}$) is the Langmuir sorption equilibrium constant, related to the affinity between an adsorbent and adsorbate, K_F (($\mu\text{mol g}^{-1}$)/($\mu\text{mol L}^{-1}$)^n) is the Freundlich equilibrium constant, and n (dimensionless) is the Freundlich intensity parameter, which indicates the magnitude of the adsorption driving force or the surface heterogeneity.

GraphPad Prism 5 was used to determine the parameters of kinetic and equilibrium models using nonlinear regression analysis. The quality of the fittings of the experimental data with the described models was evaluated by calculating the determination coefficient (R^2) and the standard deviation of residuals ($S_{y/x}$).

3. RESULTS AND DISCUSSION

3.1. Materials characterization

The efficiency of MAC towards the removal of pharmaceuticals from aqueous media relies fundamentally on a compromise between their S_{BET} and magnetic properties. Table 1 presents the textural parameters and the M_s obtained for MAC-CP and MAC-MW and their carbon (AC-CP and AC-MW, respectively) and magnetic precursors (Fe-MNP).

3.1.1. Specific surface area and textural properties

From Table 1, it is possible to infer the formation of well-developed porous structures, with the micropore volume accounting for *ca*. 57 % of total pore volume in the case of AC-CP and AC-MW, 35 % for MAC-CP and 38 % in the case of MAC-MW. The loading of Fe-MNP onto the carbon matrix led to a decrease in the S_{BET} of the produced MAC-CP and MAC-MW, by *ca*. 55 % and 50 %, respectively. These negative effects on the S_{BET} can be explained by the very low S_{BET} of the bare Fe-MNP (17 to 23 times lower than the values obtained for the AC) that was deposited on the matrix of AC-CP and AC-MW. According to the decrease in V_p and W_0 observed for both MAC (when compared to the corresponding AC precursor), the occupation of the interstitial pore spaces by nano-sized iron oxides (usually bellow 100 nm [7]) may have contributed to reduce S_{BET} of MAC-CP and MAC-MW. In any case, S_{BET} and textural properties of MAC-CP and MAC-MW are quite similar, even when they were produced from AC obtained under different conditions (as detailed in section 2.2), namely activating agent amount (AC-MW required only one fifth of the mass of KOH, compared to that required for the production of AC-CP) and pyrolysis procedure (CP or MW, with the latter

requiring residence time 7.5 times shorter). The significantly lower pyrolysis time and amount of chemical activating agent used in the MW-assisted pyrolysis to produce a material with similar textural properties of the ones obtained by conventional heating is a remarkable feature of this thermochemical process. Furthermore, the S_{BET} of MAC-CP and MAC-MW (Table 1) was comparable to values found in the literature for other MAC prepared from commercial AC (433 m^2 g^{-1} to 783 m^2 g^{-1}) [22,26,47–50].

The pore size distribution of MAC-CP and MAC-MW was also evaluated (Figure S2 in SM) and the results obtained were similar for both materials, with pore sizes ranging between 1.3 to 50 nm. A higher incidence of pores between 1.3 nm and 15 nm was observed for both MAC, but MAC-MW was the one exhibiting a larger distribution of pores within this size interval. The prevailing pores of both MAC ranged between 1.3 nm and 1.6 nm, which indicates a higher presence of micropores in their structure. Additionally, macropores of *ca.* 63 nm were detected on MAC-CP. These macropores, along with other mesopores, can be regarded as a suitable medium to access the inner microporous structure of this material.

3.1.2. Magnetic properties

Regarding the magnetic properties, the M_s of 69 emu g^{-1} found for MNP was in agreement with published values for magnetite (Fe_3O_4) and maghemite (Fe_2O_3) produced by co-precipitation, *viz.* 60 emu g^{-1} [51] and 58 emu g^{-1} [47], respectively. The incorporation of these MNP onto the matrix of the non-magnetic AC resulted in M_s of 32.9 emu g^{-1} and 22.5 emu g^{-1} for MAC-CP and MAC-MW, respectively. According to Wang *et al.* (2014), a M_s value higher than 16 emu g^{-1} [52] is indicative of an efficient magnetic separation by a permanent magnet, guaranteeing an easy recovery from aqueous medium. The differences observed on M_s values for MAC-CP and MAC-MW, bearing in

mind that in both cases it was used a 1:4 (*w/w*) AC:iron salts ratio and a 1:3 (*w/w*) $Fe^{3+}:Fe^{2+}$ ratio, can be related to the higher porosity of AC-CP when compared to that of AC-MW (according to the values of V_p and W_0 on Table 1) , which may have contributed to entrap higher levels of Fe-MNP.

3.1.3. Point of zero charge

The results from the determination of the materials pH_{PZC} are depicted in Table 1. As it may be seen, the pH_{PZC} values of MAC-CP and MAC-MW were 5.9 and 6.4, respectively, implying that the surface of both materials in the tested adsorption conditions (pH adjusted to 7.5±0.1 in UW and pH of 8.4 in EF), are mainly deprotonated and negatively charged. Regarding bare Fe-MNP, AC-CP and AC-MW used as precursors, they displayed quite similar values of pH_{PZC} (Table 1).

3.1.4. XPS analysis

The surface chemical composition of MAC-CP and MAC-MW was compared to that of their carbon precursors, i.e., AC-CP and AC-MW, respectively (Figure 1). The overall XPS spectra (Figure 1A) show two main peaks, ascribed to C 1s and O 1s core levels, while in the case of MAC-CP and MAC-MW, besides these two, Fe 2p and Fe 3s peaks were also identified. Complementary, other small peaks, namely Si 2p, Si 2s and N 1s, were also visible for all the analysed materials.

The relative abundance (atomic %) of C, O, Fe, Si and N was determined for all materials (Figure 1B). The results indicate higher contents of carbon for the AC than for the MAC materials (with an observed decrease of *ca.* 21 % for MAC-CP and 37 % for MAC-MW), which must be related to the incorporation of magnetic nanoparticles.

Contrarily, the results indicate higher oxygen and iron contents (21.8 % to 39.9 % for oxygen and 5.1 % to 12.8 % for iron) on the surface of the nanocomposite materials, resulting from the formation of iron oxides. The amount of iron detected was 8.5 % for MAC-CP and 10.8 % for MAC-MW. The occurrence of silicon in all materials, with atomic concentrations ranging between 2.5 % and 9.9 %, might be due to the specific composition of paper mill sludge, which has been shown to contain this element [53,54], mainly resulting from the removal of Si compounds (such as waterglass, $3SiO_2 \cdot Na_2O$) during wastewater treatment [55]. The amount of nitrogen was negligible and only trace amounts (<1.1 %) were detected on the surface of all materials.

Figure 2 presents the C1s, O1s and Fe2p core levels of XPS spectra of AC-CP, AC-MW, MAC-CP and MAC-MW. As it may be seen, C 1s spectra of both AC samples show a main peak with the typical asymmetric shape of graphitic like carbons and several features at Binding Energies (BE) associated to defects in the structure and diverse functional groups of oxygen linked to carbons (for further information please see Table S3 in SM). After the incorporation of iron nanoparticles, a significant contrast between the C 1s spectra of the two MAC was observed. C 1s spectrum of MAC-CP preserves a shape similar to the AC-CP precursor, while MAC-MW exhibits an evident widening when compared to AC-MW. Differences may be assessed by the respective values of full width at half maximum (FWHM). The FWHM of both AC are around 1.1 eV, which remains the same for MAC-CP but increases to 2.1 eV in the case of MAC-MW. This widening, indicates a higher weight of the C sp^3 component, suggesting a more defective surface. Besides C 1s, signals associated to potassium appear in both MAC spectra, at BE values beyond 293 eV, resulting from KOH used as activated agent in the production of the respective AC materials. Other noticeable difference is the ratio between iron and carbon of MAC, which is almost double in MAC-MW than in MAC-CP, i.e., 1:3.8 and

1:7, respectively. These divergences might indicate a different distribution of the iron particles on both MAC, due to their specific morphologies. Fe 2p spectra of both MAC showed a similar shape with a significant satellite feature near 720.0 eV, associated to Fe^{3+} oxidation state. The incorporation of iron particles is also reflected in the O 1s spectra of both MAC composites, mainly through the emergence of a component related to oxygen linked to iron, centred at 530.3 eV for MAC-CP and 530.5 eV for MAC-MW.

3.2. Adsorption studies

3.2.1. Kinetic adsorption studies

The kinetic curves (q_t *vs* t) of DCF and VEN adsorption onto MAC-CP and MAC-MW in UW and EF from WWTP were established, allowing to evaluate the time required to attain the equilibrium (t_{eq}) between the aqueous and the solid phases. Figure 3 shows the experimental data and the corresponding fittings with kinetic surface reaction models; the experimental and fitted parameters for each system are listed in Table 2.

As it may be seen in Figure 3, the kinetic profiles obtained for MAC-CP with DCF and VEN in both UW and EF matrices are described by an abrupt increase of q_t values up to t~30 min, representing the rapid uptake of these two pharmaceuticals from aqueous media until approaching equilibrium. Regarding MAC-MW, the initial slope of the kinetic profile was less steep than for MAC-CP in the case of DCF adsorption in UW, also attaining a lower q_t value at the equilibrium. Meanwhile, the remaining MAC-MW systems followed more similar trends to those of MAC-CP. For all the studied systems, equilibrium was attained within 60 min. An analogous equilibrium time (*ca.* 60 minutes) was reported by Calisto et al. (2015) for the removal of VEN by commercial AC, within identical experimental conditions [56]. No information has been found regarding the adsorption of VEN by MAC. For DCF, according to the information in the literature,

longer equilibrium times are needed (t_{eq} ranging from 3 to 24 h) for its removal by both MAC [57] and commercial AC [58,59]. However, in those studies the experimental conditions used, namely the adsorbent dose (200 to 400 mg L^{-1}) and DCF initial concentration (157 to 314 µmol L^{-1}), were not comparable to those of the present work. Other studies highlight that the incorporation of magnetic Fe-MNP onto AC surface does not affect the time needed to reach equilibrium, determining identical t_{eq} for AC and MAC [23,48].

The fittings of the experimental kinetic results showed a good agreement between the experimental data and both P1O and P2O theoretical models, with R^2 values above 0.98 (Table 2). Furthermore, the lower $S_{y/x}$ typically obtained for the P2O model suggests a better fitting to the experimental data. The P2O reaction rate constants showed a superior kinetic efficiency for MAC-CP, with k_2 values being 1.4 to 2.9 times higher than those obtained for MAC-MW. Furthermore, the adsorption rate of DCF by MAC-CP was alike in both EF and UW, but it was faster in EF for MAC-MW. For VEN, MAC-CP exhibited a faster adsorption in EF when compared with that in UW, and MAC-MW showed close adsorption rate constants in both EF and UW. The predicted q_e ($q_{e\ fit}$) from P1O and P2O models were in agreement with the experimental values ($q_{e\ exp}$), relative errors being between 0.01 % and 9.3 %.

3.2.2. Equilibrium adsorption studies

The distribution of DCF and VEN between the aqueous and the solid phases of MAC-CP and MAC-MW, in both UW and EF was evaluated by collecting the data from the equilibrium experiments and by fitting the non-linear Langmuir and Freundlich models (Figure 4). The equilibrium fitted parameters were determined for each system (Table 3), providing information on the affinity and capacity of both MAC.

The analysis of Figure 4 shows that both Langmuir and Freundlich models provide good fittings across the studied concentration range. This may be confirmed by R^2 close to unit, which are all ≥ 0.98 (Table 3), with values corresponding to Langmuir model being slightly higher for most systems. The lower $S_{y/x}$ values obtained with Langmuir isotherm for the majority of the systems studied corroborate these results.

A complete monolayer coverage with values ranging from 97 ± 2 µmol g^{-1} to 215 ± 4 µmol g^{-1} was obtained for MAC-CP, and from 80 ± 2 µmol g^{-1} to 172 ± 3 µmol g^{-1} for MAC-MW. Typically, the values of the maximum adsorption capacity (q_m) attained by MAC-CP were higher (17 % to 56 %) than those obtained by MAC-MW, except for the equilibrium studies with VEN in UW, where q_m were quite similar (difference of $ca.$ 6 %). Besides that, for both adsorbents, the q_m decreased in EF as compared with UW (q_m is 15 % to 55 % lower), suggesting the existence of matrix effects.

Evaluating the affinity constant between the adsorbent and adsorbate (K_L), the highest values obtained for VEN in both water matrices suggest that MAC-CP and MAC-MW have a higher affinity for this pharmaceutical than for DCF. Considering the ionizable properties of VEN and DCF, these compounds can establish electrostatic interactions with the adsorbent materials depending on the pK_a (affecting their speciation), the solution pH and the pH$_{PZC}$ of MAC. As discussed in section 3.1 and based on the pH$_{PZC}$ (Table 1), the surface of MAC-CP and MAC-MW was negatively charged under the tested conditions (pH 7.5 ± 0.1 in UW and 8.42 in EF). Given the value of pK_a of 4.15 [60,61] for DCF (Table S2 of SM), this pharmaceutical was mainly in its negative form [62] in either UW or EF. Consequently, other types of mechanisms, rather than electrostatic interactions, might be controlling the adsorption process, namely electron donor–acceptor interactions between the polar aromatic DCF and the polarizable MAC (which might act as electron donors due to their highly aromatic nature). As for VEN,

considering the pk$_{a1}$ of 8.91 and pk$_{a2}$ of 14.42 [63] (Table S2 of SM), this compound was mainly cationic in the experiments performed in UW, while in EF both cationic and neutral forms (*ca.* 75 % and 25 %, respectively) were in solution. For this reason, electrostatic interactions must have had a relevant role in the adsorption of VEN onto MAC-CP and MAC-MW and are a possible explanation for the higher K_L values obtained for this pharmaceutical as compared to DCF.

3.2.3. Competitive adsorption studies

Figure 5 presents the results from the experiments described in section 2.6.3, namely the adsorption percentages of DCF and VEN in MAC-CP and MAC-MW in binary and single solutions.

In general, a decrease in the percentage of removal occurred in binary solutions, which could be explained by the competition among the pharmaceuticals for the active sites on either MAC-CP or MAC-MW. Other works in the literature also verified a decrease in the removal efficiency in multi-component systems (using other pharmaceuticals) with MAC [64,65]. In addition, results in Figure 5 show that the overall impact of competition on the adsorbed concentration was mostly higher for MAC-MW (except for DCF in UW), leading to a decrease of 23 % to 62 % in the adsorption percentages. For MAC-CP, the impact in the adsorption percentage values derived from the simultaneous presence of DCF and VEN in solution was lower (the decrease does not exceed 42 %), which may be related to the higher S_{BET} of this material and/or the type of mechanisms involved in the adsorption process. Still, in some of the studied systems, such as the removal of DCF (from EF) onto MAC-CP and VEN (from UW) onto MAC-CP, the adsorption percentages in the binary and single systems were analogous.

3.2.4. Regeneration and reutilization

MW-assisted irradiation was used as a tool to regenerate exhausted MAC-CP and MAC-MW. Prior to the selection of MW temperature, the thermogravimetric profiles of both pharmaceuticals were evaluated (see Figure S1 in SM). Considering the obtained results, the MW regeneration tests were conducted at 400 ºC and using a residence time of 20 min.

Figure 6 depicts the results from reutilization experiments described in section 2.6.4., namely the adsorption percentages of DCF and VEN (from single or binary solutions in UW) onto the regenerated MAC-CP and MAC-MW (2nd adsorption cycle) as compared with the virgin materials (1st adsorption cycle). No significant differences (with 95 % confidence level) were observed between the 2nd and the 1st adsorption cycles for the adsorption percentage of DCF and VEN in single solutions by both MAC. Meanwhile, in binary solutions, a small decrease was observed in the adsorption percentage of DCF and VEN for MAC-CP (*ca.* 1.5-1.6 times) but not for MAC-MW. These results highlight the feasibility of the MW-assisted regeneration of saturated MAC-CP and MAC-MW and indicates that it did not affect the adsorptive performance of the materials. In line with the here obtained results, some studies verified that the porous structure of carbon-based adsorbents, exhausted with organic contaminants, is preserved after MW heating regeneration [29–31], being one of the highlighted advantages of this regeneration process in comparison with regeneration by conventional treatment. Also, in the present work, the magnetic response of the regenerated materials was not visually affected by regeneration, indicating that the retrievability of the recycled material was preserved. Thus, MW-assisted heating revealed to be a feasible process in the regeneration of MAC, so representing an attractive alternative to conventional heating and/or chemical processes.

3.2.5. MAC's surface chemistry after adsorption saturation and regeneration

To gather information on the surface chemistry of MAC-CP and MAC-MW after adsorption with DCF and MW-assisted regeneration processes (experiments described in section 2.3.4), XPS analysis was performed. DCF was also analyzed for comparison purposes. The overview spectrum of DCF (Figure S3 depicted in SM) showed C 1s, O 1s, Cl 2p, Na 1s and N 1s peaks, as expected from its molecular structure (please see Table S2 in SM).

In the case of saturated MAC-CP after the 1st adsorption cycle, the presence of chlorine, which exists in the DCF molecule, was confirmed by XPS (Figure S4 in SM). In fact, Cl 2p$_{3/2}$ peak appears at the same BE than that of DCF, 200.5 eV, assigned to C$_x$-Cl species. Furthermore, the analysis of C 1s spectrum of MAC-CP after DCF adsorption (Figure S5 in SM) indicates a higher contribution of the peaks assigned to C-O and O=C-O, centred at 286.2 and 289.1 eV, respectively. This might indicate the presence of the pharmaceutical through the C=C-Cl and O=C-O functionalities, respectively. On the other hand, regarding MAC-MW, XPS was not able to detect chlorine after the adsorption experiments (despite the removal observed in adsorption experiments), which could be due to the amount of chlorine being under the detection limit of the equipment or hidden at the surface due to the highly microporous structure of MAC-MW. Furthermore, no significant changes were observed in C 1s and Fe 2p spectrum (Figure S5 in SM).

Regarding the chemical surface of MAC after the MW-assisted regeneration, Cl 2p was detected in both regenerated MAC, the main Cl 2p$_{3/2}$ peak at 198.6 eV (Figure S4 in SM). This BE, almost 2 eV lower than the detected in the molecule, points to metal linked Cl, most probably NaCl, since Na 1s was also detected in both samples (Figure S4 in SM), which arises from the DCF formulation used in this study (diclofenac sodium

salt). In good agreement with this, Na 1s spectra of the regenerated MAC appear shifted at higher BE with respect to the one measured for the pharmaceutical, approximately 1072 eV *vs* 1071.2 eV, respectively. These data suggest a partial cleavage of the DCF molecule during MW regeneration and the consequent presence of residual NaCl. Furthermore, the presence of Cl 2p peaks on regenerated MAC-MW suggests the existence of hidden DCF in the porous structure of the sample after the 1st cycle of adsorption experiments. A possible restructuration of MAC-MW surface by MW-assisted regeneration could be the cause for uncovering DCF. On the other hand, C 1s and Fe 2p spectra (Figure S5) do not reflect any relevant negative impact neither on the surfaces of the carbonaceous matrix nor on the iron particles. These results reinforce that, after one MW regeneration step, both MAC maintained their magnetic and surface chemical characteristics.

4. CONCLUSIONS

In the present work, two composite MAC (MAC-MW and MAC-CP) with satisfactory S_{BET} (548 and 644 m^2 g^{-1}, respectively) were produced by loading magnetic iron oxides onto waste-based AC obtained by two thermochemical methods. Both MAC were efficiently applied in the removal of DCF and VEN from ultrapure water and WWTP effluent. Their magnetic features (M_s of 22.5 and 32.9 emu g^{-1} for MAC-MW and MAC-CP, respectively), allowed an easy after-use separation and recovery of the exhausted material from the solution. The kinetic profile of each studied system indicated that equilibrium was quickly attained in both ultrapure and WWTP effluent ($t_{eq} \leq 60$ min). For equilibrium results, Langmuir fittings showed that q_m were mostly higher for MAC-CP, varying between 97±2 and 215±4 µmol g^{-1}, compared to values between 80±2 and 172±3 µmol g^{-1} for MAC-MW. The adsorption of DCF and VEN onto both MAC was inhibited due to competitive effects (either in binary solutions or in WWTP effluent).

Finally, MW-assisted heating was effective in the regeneration of saturated MAC-CP and MAC-MW, without affecting their adsorptive performance and surface chemical features. Overall, this study points out the viability of producing waste-derived iron-carbon composites combining high efficiency for DCF and VEN adsorptive removal with easy retrievability and successful regeneration/reutilization.

Acknowledgements

References

[1]   S. Fekadu, E. Alemayehu, R. Dewil, B. Van der Bruggen, Pharmaceuticals in freshwater aquatic environments: A comparison of the African and European challenge, Sci. Total Environ. 654 (2019) 324–337. https://doi.org/10.1016/j.scitotenv.2018.11.072.

[2]   M. Patel, R. Kumar, K. Kishor, T. Mlsna, C.U. Pittman, D. Mohan, Pharmaceuticals of

emerging concern in aquatic systems: Chemistry, occurrence, effects, and removal

methods, Chem. Rev. 119 (2019) 3510–3673.

https://doi.org/10.1021/acs.chemrev.8b00299.

[3]   S. Comber, M. Gardner, P. Sörme, D. Leverett, B. Ellor, Active pharmaceutical

ingredients entering the aquatic environment from wastewater treatment works: A cause

for concern?, Sci. Total Environ. 613–614 (2018) 538–547.

https://doi.org/10.1016/j.scitotenv.2017.09.101.

[4]   J.R. De Andrade, M.F. Oliveira, M.G.C. Da Silva, M.G.A. Vieira, Adsorption of

Pharmaceuticals from Water and Wastewater Using Nonconventional Low-Cost

Materials: A Review, Ind. Eng. Chem. Res. 57 (2018) 3103–3127.

https://doi.org/10.1021/acs.iecr.7b05137.

[5]   Directive 2013/39/EU of the European Parliament and of the Council of 12 August 2013

amending Directives 2000/60/EC and 2008/105/EC as regards priority substances in the

field of water policy. Brussels, 2013.

[6]   L. Rizzo, S. Malato, D. Antakyali, V.G. Beretsou, M.B. Đolić, W. Gernjak, E. Heath, I.

Ivancev-Tumbas, P. Karaolia, A.R. Lado Ribeiro, G. Mascolo, C.S. McArdell, H.

Schaar, A.M.T. Silva, D. Fatta-Kassinos, Consolidated vs new advanced treatment

methods for the removal of contaminants of emerging concern from urban wastewater,

Sci. Total Environ. 655 (2019) 986–1008.

https://doi.org/10.1016/j.scitotenv.2018.11.265.

[7]   L.S. Rocha, D. Pereira, É. Sousa, M. Otero, V.I. Esteves, V. Calisto, Recent advances on

the development and application of magnetic activated carbon and char for the removal

of pharmaceutical compounds from waters: A review, Sci. Total Environ. 718 (2020)

137272. https://doi.org/10.1016/j.scitotenv.2020.137272.

[8]   K.R. Thines, E.C. Abdullah, N.M. Mubarak, M. Ruthiraan, Synthesis of magnetic

biochar from agricultural waste biomass to enhancing route for waste water and polymer

application: A review, Renew. Sustain. Energy Rev. 67 (2017) 257–276.

https://doi.org/10.1016/j.rser.2016.09.057.

[9]   H. Ma, J.B. Li, W.W. Liu, M. Miao, B.J. Cheng, S.W. Zhu, Novel synthesis of a versatile magnetic adsorbent derived from corncob for dye removal, Bioresour. Technol. 190 (2015) 13–20. https://doi.org/10.1016/j.biortech.2015.04.048.

[10]   F. Mansour, M. Al-Hindi, R. Yahfoufi, G.M. Ayoub, M.N. Ahmad, The use of activated carbon for the removal of pharmaceuticals from aqueous solutions: a review, Rev. Environ. Sci. Biotechnol. 17 (2018) 109–145. https://doi.org/10.1007/s11157-017-9456-8.

[11]   R.K. Liew, E. Azwar, P.N.Y. Yek, X.Y. Lim, C.K. Cheng, J.H. Ng, A. Jusoh, W.H. Lam, M.D. Ibrahim, N.L. Ma, S.S. Lam, Microwave pyrolysis with KOH/NaOH mixture activation: A new approach to produce micro-mesoporous activated carbon for textile dye adsorption, Bioresour. Technol. 266 (2018) 1–10. https://doi.org/10.1016/j.biortech.2018.06.051.

[12]   W. Ao, J. Fu, X. Mao, Q. Kang, C. Ran, Y. Liu, H. Zhang, Z. Gao, J. Li, G. Liu, J. Dai, Microwave assisted preparation of activated carbon from biomass: A review, Renew. Sustain. Energy Rev. 92 (2018) 958–979. https://doi.org/10.1016/j.rser.2018.04.051.

[13]   H. Huang, S. Zhou, C. Yu, H. Huang, J. Zhao, L. Dai, J. Qiu, Rapid and energy-efficient microwave pyrolysis for high-yield production of highly-active bifunctional electrocatalysts for water splitting, Energy Environ. Sci. 13 (2020) 545–553. https://doi.org/10.1039/c9ee03273h.

[14]   M.A. Chayid, M.J. Ahmed, Amoxicillin adsorption on microwave prepared activated carbon from Arundo donax Linn: Isotherms, kinetics, and thermodynamics studies, J. Environ. Chem. Eng. 3 (2015) 1592–1601. https://doi.org/10.1016/j.jece.2015.05.021.

[15]   M.J. Ahmed, S.K. Theydan, Microporous activated carbon from Siris seed pods by microwave-induced KOH activation for metronidazole adsorption, J. Anal. Appl. Pyrolysis. 99 (2013) 101–109. https://doi.org/10.1016/j.jaap.2012.10.019.

[16]   R.A. Reza, M. Ahmaruzzaman, A.K. Sil, V.K. Gupta, Comparative adsorption behavior of ibuprofen and clofibric acid onto microwave assisted activated bamboo waste, Ind. Eng. Chem. Res. 53 (2014) 9331–9339. https://doi.org/10.1021/ie404162p.

[17]   É. Sousa, L. Rocha, G. Jaria, M. V Gil, M. Otero, V.I. Esteves, V. Calisto, Optimizing microwave-assisted production of waste-based activated carbons for the removal of antibiotics from water, Sci. Total Environ. 752 (2021) 141662. https://doi.org/10.1016/j.scitotenv.2020.141662.

[18]   H. Huang, C. Yu, H. Huang, W. Guo, M. Zhang, X. Han, Q. Wei, S. Cui, X. Tan, J. Qiu, Microwave-Assisted Ultrafast Synthesis of Molybdenum Carbide Nanoparticles Grown on Carbon Matrix for Efficient Hydrogen Evolution Reaction, Small Methods. 3 (2019) 1–7. https://doi.org/10.1002/smtd.201900259.

[19]   Z. Wang, C. Yu, H. Huang, W. Guo, C. Zhao, W. Ren, Y. Xie, J. Qiu, Energy Accumulation Enabling Fast Synthesis of Intercalated Graphite and Operando Decoupling for Lithium Storage, Adv. Funct. Mater. 2009801 (2021) 2009801. https://doi.org/10.1002/adfm.202009801.

[20]   M.T.H. Siddiqui, S. Nizamuddin, H.A. Baloch, N.M. Mubarak, M. Al-Ali, S.A. Mazari, A.W. Bhutto, R. Abro, M. Srinivasan, G. Griffin, Fabrication of advance magnetic carbon nano-materials and their potential applications: A review, J. Environ. Chem. Eng. 7 (2019). https://doi.org/10.1016/j.jece.2018.102812.

[21]   S. Wong, N. Ngadi, I.M. Inuwa, O. Hassan, Recent advances in applications of activated carbon from biowaste for wastewater treatment: A short review, J. Clean. Prod. 175 (2018) 361–375. https://doi.org/10.1016/j.jclepro.2017.12.059.

[22]   J. Wan, H.P. Deng, J. Shi, L. Zhou, T. Su, Synthesized magnetic manganese ferrite nanoparticles on activated carbon for sulfamethoxazole removal, Clean - Soil, Air, Water. 42 (2014) 1199–1207. https://doi.org/10.1002/clen.201300432.

[23]   P. Rai, K.P. Singh, Valorization of Poly (ethylene) terephthalate (PET) wastes into magnetic carbon for adsorption of antibiotic from water: Characterization and application, J. Environ. Manage. 207 (2018) 249–261. https://doi.org/10.1016/j.jenvman.2017.11.047.

[24]   M.Y. Badi, A. Azari, H. Pasalari, A. Esrafili, M. Farzadkia, Modification of activated carbon with magnetic Fe3O4 nanoparticle composite for removal of ceftriaxone from

aquatic solutions, J. Mol. Liq. 261 (2018) 146–154.

https://doi.org/10.1016/j.molliq.2018.04.019.

[25] S.T. Danalıoğlu, Ş.S. Bayazit, Ö. Kerkez Kuyumcu, M.A. Salam, Efficient removal of

antibiotics by a novel magnetic adsorbent: Magnetic activated carbon/chitosan (MACC)

nanocomposite, J. Mol. Liq. 240 (2017) 589–596.

https://doi.org/10.1016/j.molliq.2017.05.131.

[26] K.T. Wong, Y. Yoon, S.A. Snyder, M. Jang, Phenyl-functionalized magnetic palm-based

powdered activated carbon for the effective removal of selected pharmaceutical and

endocrine-disruptive compounds, Chemosphere. 152 (2016) 71–80.

https://doi.org/10.1016/j.chemosphere.2016.02.090.

[27] J. Oladejo, K. Shi, Y. Chen, X. Luo, Y. Gang, T. Wu, Closing the active carbon cycle:

Regeneration of spent activated carbon from a wastewater treatment facility for resource

optimization, Chem. Eng. Process. - Process Intensif. 150 (2020).

https://doi.org/10.1016/j.cep.2020.107878.

[28] K.Y. Foo, B.H. Hameed, A cost effective method for regeneration of durian shell and

jackfruit peel activated carbons by microwave irradiation, Chem. Eng. J. 193–194 (2012)

404–409. https://doi.org/10.1016/j.cej.2012.04.055.

[29] C.O. Ania, J.B. Parra, J.A. Menéndez, J.J. Pis, Effect of microwave and conventional

regeneration onthe microporous and mesoporous network and on theadsorptive capacity

of activated carbons, Microporous Mesoporous Mater. 85 (2005) 7–15.

[30] C.O. Ania, J.B. Parra, J.A. Menéndez, J.J. Pis, Microwave-assisted regeneration of

activated carbons loaded with pharmaceuticals, Water Res. 41 (2007) 3299–3306.

https://doi.org/10.1016/j.watres.2007.05.006.

[31] C. Cui, Q. Zheng, Y. Han, Y. Xin, Rapid microwave-assisted regeneration of magnetic

carbon nanotubes loaded with p-nitrophenol, Appl. Surf. Sci. 346 (2015) 99–106.

https://doi.org/10.1016/j.apsusc.2015.03.212.

[32] K.Y. Foo, B.H. Hameed, Microwave-assisted regeneration of activated carbon,

Bioresour. Technol. 119 (2012) 41–47. https://doi.org/10.1016/j.biortech.2012.05.061.

[33]   M. Wang, X.L. Wang, G.Q. Gao, Research on the regeneration of modified activated carbon containing 2,4,6-TCP by microwave irradiation, Adv. Mater. Res. 1033–1034 (2014) 1358–1361. https://doi.org/10.4028/www.scientific.net/AMR.1033-1034.1358.

[34]   G. Jaria, C. Patrícia, J.A.B.P. Oliveira, S.M. Santos, M. Victoria, M. Otero, V. Calisto, V.I. Esteves, Production of highly efficient activated carbons from industrial wastes for the removal of pharmaceuticals from water — A full factorial design, J. Hazard. Mater. 370 (2019) 212–218. https://doi.org/10.1016/j.jhazmat.2018.02.053.

[35]   Decision (EU) 2015/495 of 20 March 2015 establishing a watch list of substances for Union-wide monitoring in the field of water policy pursuant to Directive 2008/105/EC of the European Parliament and of the Council. Brussels, 2015.

[36]   Decision (EU) 2020/1161 of 4 August 2020 establishing a watch list of substances for Union-wide monitoring in the field of water policy pursuant to Directive 2008/105/EC of the European Parliament and of the Council. Brussels, 2020.

[37]   Directive 2000/60/EC of the European Parliament and of the Council of 23 October 2000 establishing a framework for Community action in the field of water policy. Brussels, 2000.

[38]   G. Jaria, C. Patrícia, C.I.A. Ferreira, M. Otero, Sludge from paper mill ef fl uent treatment as raw material to produce carbon adsorbents : An alternative waste management strategy, 188 (2017) 203–211. https://doi.org/10.1016/j.jenvman.2016.12.004.

[39]   L.S. Rocha, É.M.L. Sousa, M.V. Gil, J.A.B.P. Oliveira, M. Otero, V.I. Esteves, V. Calisto, Producing Magnetic Nanocomposites from Paper Sludge for the Adsorptive Removal of Pharmaceuticals from Water—A Frac-tional Factorial Design, Nanomaterials. 11 (2021).

[40]   S. Brunauer, P.H. Emmett, E. Teller, Adsorption of Gases in Multimolecular Layers, J. Am. Chem. Soc. 60 (1938) 309–319. https://doi.org/10.1021/ja01269a023.

[41]   B. Rand, H. Marsh, The process of activation of carbons by gasification with CO2-I. Gasification of pure polyfurfuryl alcohol carbon, Carbon N. Y. 9 (1971) 47–61.

https://doi.org/10.1016/0008-6223(71)90145-X.

[42]   V. Calisto, C.I.A. Ferreira, S.M. Santos, M.G. Victoria, M. Otero, V.I. Esteves, Production of adsorbents by pyrolysis of paper mill sludge and application on the removal of citalopram from water, Bioresour. Technol. 166 (2014) 335–344. https://doi.org/10.1016/j.biortech.2014.05.047.

[43]   S. Lagergren, Zur theorie der sogenannten adsorption geloster stoffe. 24:1–39, K. Sven. Vetenskapsakad. Handl. 24 (1898) 1–39.

[44]   Y.S. Ho, G. Mckay, Pseudo-second order model for sorption.pdf, 34 (1999) 451–465.

[45]   I. Langmuir, The adsorption of gases on plane surfaces of glass, mica and platinum, J. Am. Chem. Soc. 40 (1918) 1361–1403. https://doi.org/https://doi.org/ 10.1021/ja02242a004.

[46]   H. Freundlich, Uber die Adsorption in Losungen, Zeitschrift Für Phys. Chemie. 57 (1906) 385–470.

[47]   K.M. Lompe, S. Vo Duy, S. Peldszus, S. Sauvé, B. Barbeau, Removal of micropollutants by fresh and colonized magnetic powdered activated carbon, J. Hazard. Mater. 360 (2018) 349–355. https://doi.org/10.1016/j.jhazmat.2018.07.072.

[48]   K.T. Wong, Y. Yoon, M. Jang, Enhanced recyclable magnetized palm shell waste-based powdered activated carbon for the removal of ibuprofen: Insights for kinetics and mechanisms, PLoS One. 10 (2015) 1–18. https://doi.org/10.1371/journal.pone.0141013.

[49]   B. Kakavandi, A. Esrafili, A. Mohseni-Bandpi, A.J. Jafari, R.R. Kalantary, Magnetic Fe3O4@C nanoparticles as adsorbents for removal of amoxicillin from aqueous solution, Water Sci. Technol. 69 (2014) 147–155. https://doi.org/10.2166/wst.2013.568.

[50]   D. Shan, S. Deng, T. Zhao, B. Wang, Y. Wang, J. Huang, G. Yu, J. Winglee, M.R. Wiesner, Preparation of ultrafine magnetic biochar and activated carbon for pharmaceutical adsorption and subsequent degradation by ball milling, J. Hazard. Mater. 305 (2016) 156–163. https://doi.org/10.1016/j.jhazmat.2015.11.047.

[51]   M. Baghdadi, E. Ghaffari, B. Aminzadeh, Removal of carbamazepine from municipal wastewater effluent using optimally synthesized magnetic activated carbon: Adsorption

and sedimentation kinetic studies, J. Environ. Chem. Eng. 4 (2016) 3309–3321.
https://doi.org/10.1016/j.jece.2016.06.034.

[52]   S.Y. Wang, Y.K. Tang, K. Li, Y.Y. Mo, H.F. Li, Z.Q. Gu, Combined performance of
        biochar sorption and magnetic separation processes for treatment of chromium-contained
        electroplating wastewater, Bioresour. Technol. 174 (2014) 67–73.
        https://doi.org/10.1016/j.biortech.2014.10.007.

[53]   F. Mohammadkazemi, Papermaking waste sludge fiber-cement composite panel:
        Stabilization and solidification of high fe and ti content- petrochemical ash, Cerne. 24
        (2018) 303–311. https://doi.org/10.1590/01047760201824042579.

[54]   V.P. Zambare, L.P. Christopher, Integrated biorefinery approach to utilization of pulp
        and paper mill sludge for value-added products, J. Clean. Prod. 274 (2020).
        https://doi.org/10.1016/j.jclepro.2020.122791.

[55]   T.S. Huuha, T.A. Kurniawan, M.E.T. Sillanpää, Removal of silicon from pulping
        whitewater using integrated treatment of chemical precipitation and evaporation, Chem.
        Eng. J. 158 (2010) 584–592. https://doi.org/10.1016/j.cej.2010.01.058.

[56]   V. Calisto, C.I.A. Ferreira, J.A.B.P. Oliveira, M. Otero, V.I. Esteves, Adsorptive
        removal of pharmaceuticals from water by commercial and waste-based carbons, J.
        Environ. Manage. 152 (2015) 83–90. https://doi.org/10.1016/j.jenvman.2015.01.019.

[57]   H. Luo, Y. Zhang, Y. Xie, Y. Li, M. Qi, R. Ma, S. Yang, Y. Wang, Iron-rich
        microorganism-enabled synthesis of magnetic biocarbon for efficient adsorption of
        diclofenac from aqueous solution, Bioresour. Technol. 282 (2019) 310–317.
        https://doi.org/10.1016/j.biortech.2019.03.028.

[58]   B.N. Bhadra, P.W. Seo, S.H. Jhung, Adsorption of diclofenac sodium from water using
        oxidized activated carbon, Chem. Eng. J. 301 (2016) 27–34.
        https://doi.org/10.1016/j.cej.2016.04.143.

[59]   M. Bernardo, S. Rodrigues, N. Lapa, I. Matos, F. Lemos, M.K.S. Batista, A.P. Carvalho,
        I. Fonseca, High efficacy on diclofenac removal by activated carbon produced from
        potato peel waste, Int. J. Environ. Sci. Technol. 13 (2016) 1989–2000.

https://doi.org/10.1007/s13762-016-1030-3.

[60]   A.I. Moral-Rodríguez, R. Leyva-Ramos, C.O. Ania, R. Ocampo-Pérez, E.D. Isaacs-Páez, D.H. Carrales-Alvarado, J.B. Parra, Tailoring the textural properties of an activated carbon for enhancing its adsorption capacity towards diclofenac from aqueous solution, Environ. Sci. Pollut. Res. 26 (2019) 6141–6152. https://doi.org/10.1007/s11356-018-3991-x.

[61]   F.M.O. Medina, M.B. Aguiar, M.E. Parolo, M.J. Avena, Insights of competitive adsorption on activated carbon of binary caffeine and diclofenac solutions, J. Environ. Manage. 278 (2021) 111523. https://doi.org/10.1016/j.jenvman.2020.111523.

[62]   H. Cheng, D. Song, H. Liu, J. Qu, Permanganate oxidation of diclofenac: The pH-dependent reaction kinetics and a ring-opening mechanism, Chemosphere. 136 (2015) 297–304. https://doi.org/10.1016/j.chemosphere.2014.11.062.

[63]   D.L.D. Lima, C.P. Silva, M. Otero, Dispersive liquid-liquid microextraction for the quantification of venlafaxine in environmental waters, J. Environ. Manage. 217 (2018) 71–77.

[64]   V. Arya, L. Philip, Adsorption of pharmaceuticals in water using Fe3O4 coated polymer clay composite, Microporous Mesoporous Mater. 232 (2016) 273–280. https://doi.org/10.1016/j.micromeso.2016.06.033.

[65]   F. Reguyal, A.K. Sarmah, Adsorption of sulfamethoxazole by magnetic biochar: Effects of pH, ionic strength, natural organic matter and 17α-ethinylestradiol, Sci. Total Environ. 628–629 (2018) 722–730. https://doi.org/10.1016/j.scitotenv.2018.01.323.

TABLES

Table 1. Specific surface area (S_{BET}), textural properties (total pore volume V_p, micropore volume W_0, average micropore width L, and average pore diameter D), saturation magnetization (M_s) and point of zero charge (pH_{PZC}) of the produced materials.

Material	N$_2$ adsorption at −196 °C					M_s	pH_{PZC}
	S_{BET} (m^2 g^{-1})	V_p (cm^3 g^{-1})	W_0 (cm^3 g^{-1})	L (nm)	D (nm)		
Fe-MNP	62	0.29	0.02	-	9.33	68.9	5.6
AC-CP	1438	1.00	0.57	-	1.39	0.03	5.4
MAC-CP	644	0.66	0.25	1.39	2.05	32.9	5.9
AC-MW	1085	0.73	0.42	1.10	1.35	0.00	5.0
MAC-MW	548	0.60	0.21	0.98	2.18	22.5	6.4

Table 2. Experimental data ($q_{e\ exp}$) and fitting parameters of pseudo-first order (P1O) and pseudo-second order (P2O) kinetic reaction-based models regarding the adsorption of DCF and VEN on MAC-CP and MAC-MW in ultrapure water (UW) and effluent (EF).

			$q_{e\ exp}$ ($\mu mol\ g^{-1}$)	P1O				P2O			
				$q_{e\ fit}$ ($\mu mol\ g^{-1}$)	k_1 ($\times 10^{-1}\ min^{-1}$)	R^2	$S_{y/x}$	$q_{e\ fit}$ ($\mu mol\ g^{-1}$)	k_2 ($\times 10^{-3}\ g\ \mu mol^{-1}\ min^{-1}$)	R^2	$S_{y/x}$
DCF	UW	MAC-CP	210±2	205±4	2.2±0.3	0.984	9.59	215±2	2.0±0.2	0.998	3.53
		MAC-MW	104±5	105±2	0.62±0.04	0.993	3.63	117±4	0.68±0.01	0.989	4.52
	EF	MAC-CP	80±1	79±2	1.3±0.1	0.987	3.48	84±2	2.6±0.3	0.992	2.73
		MAC-MW	70±1	70±1	0.87±0.05	0.995	2.03	77±4	1.6±0.4	0.967	5.18
VEN	UW	MAC-CP	147±2	147±3	1.2±0.1	0.987	6.24	157±2	1.2±0.1	0.998	2.42
		MAC-MW	167±2	165±4	1.0±0.1	0.988	6.83	177±4	0.9±0.1	0.991	6.10
	EF	MAC-CP	113 ±1	112±3	1.8±0.2	0.979	6.03	117±2	2.8±0.5	0.990	4.15
		MAC-MW	110±1	109±2	0.93±0.07	0.989	4.34	118±2	1.1±0.1	0.996	2.64

Table 3. Fitting parameters corresponding to the Langmuir and Freundlich equilibrium isotherm models for the adsorption of DCF and VEN with MAC-CP and MAC-MW in both ultrapure water (UW) and effluent (EF).

			Langmuir				Freundlich			
			q_m ($\mu mol\ g^{-1}$)	K_L ($L\ \mu mol^{-1}$)	R^2	$S_{y/x}$	K_F ($\mu mol^{1-1/n}\ L^{1/n}\ g^{-1}$)	n	R^2	$S_{y/x}$
DCF	UW	MAC-CP	215±4	1.2±0.1	0.994	5.4	129±6	0.19	0.983	9.0
		MAC-MW	94±1	1.9±0.1	0.997	1.6	68±2	0.12	0.990	2.8
	EF	MAC-CP	97±2	3.2±0.7	0.988	3.6	77±2	0.10	0.990	3.3
		MAC-MW	80±2	2.1±0.3	0.992	2.2	61±2	0.10	0.984	3.2
VEN	UW	MAC-CP	162±3	3.3±0.6	0.992	5.4	125±4	0.11	0.992	5.3
		MAC-MW	172±3	3.3±0.6	0.994	4.8	138±5	0.08	0.991	5.8
	EF	MAC-CP	132±3	6±2	0.985	5.6	109±1	0.10	0.999	1.9
		MAC-MW	105±2	3.7±0.6	0.993	3.1	82±3	0.11	0.980	5.2
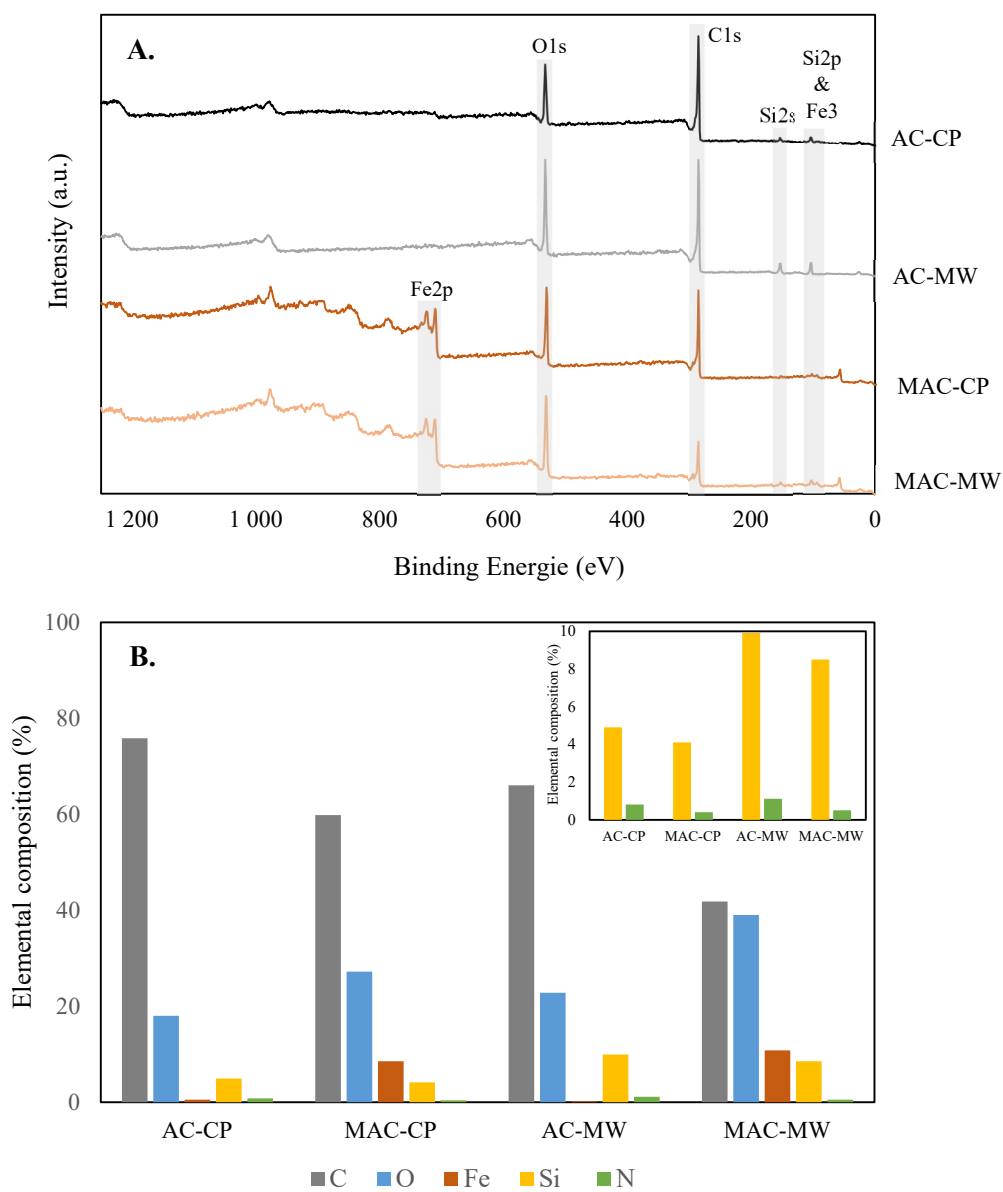
Figure 1. (A) XPS overview spectra and (B) relative atomic abundance of C, O, Fe, Si and N (expressed as %) for AC-CP, AC-MW, MAC-CP and MAC-MW.
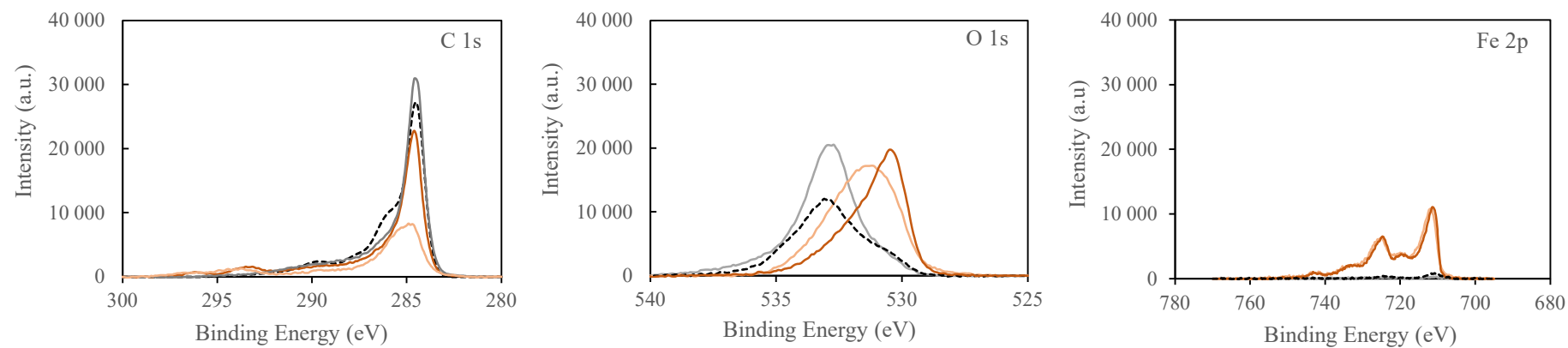
Figure 2. Comparison of the C 1s, O 1s and Fe 2p core levels of XPS spectra obtained for AC-CP (- - -) and AC-MW (——), with those of and MAC-CP (——) and MAC-MW (——).
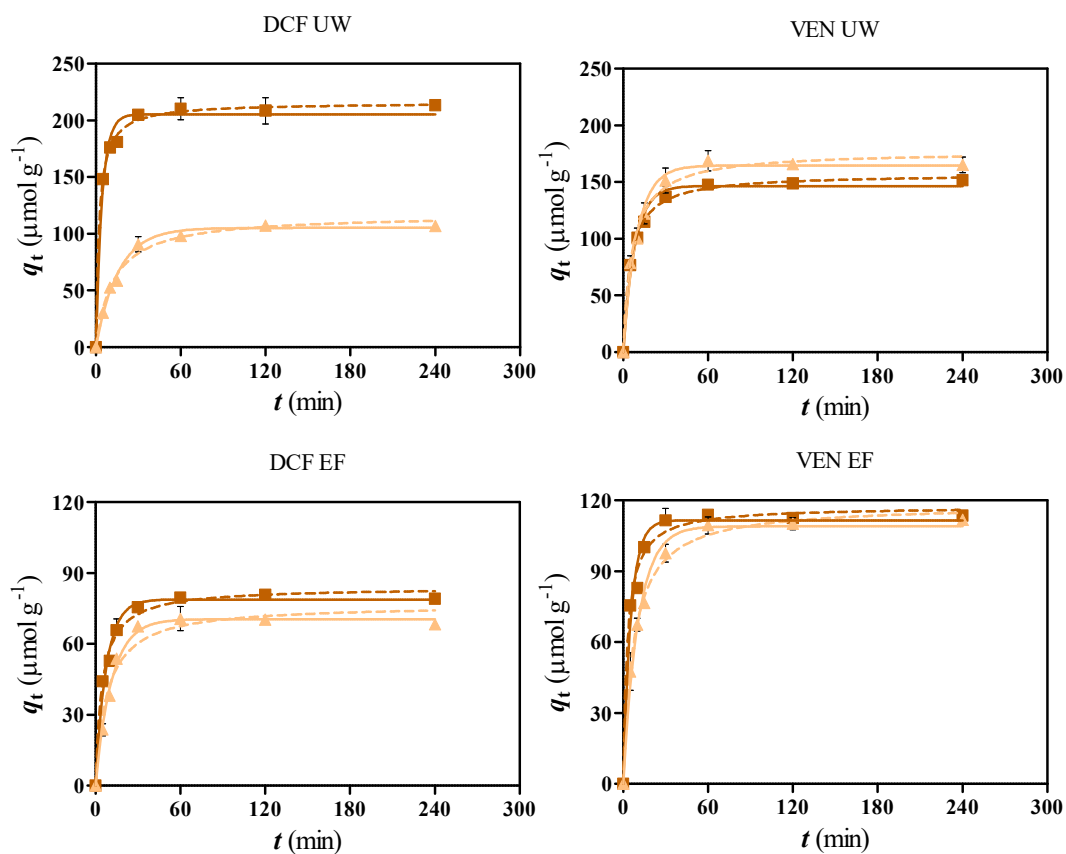
Figure 3. Kinetic data obtained for DCF and VEN in UW and EF using MAC-CP (■) and MAC-MW (▲), together with the fitting using P1O (continuous lines, — and —) and P2O (dashed lines, --- and ---) models. Experimental conditions: C_i =14 µmol L^{-1} (DCF or VEN), dose of MAC of 35 mg L^{-1} in UW (pH adjusted to 7.5±0.1) and 85 mg L^{-1} in EF (pH *ca.* 8.4). Note that *yy*-axis scale is different for UW and EF to allow a better visualization of results. Data points are the average of three independent experiments, with error bars representing standard deviations.
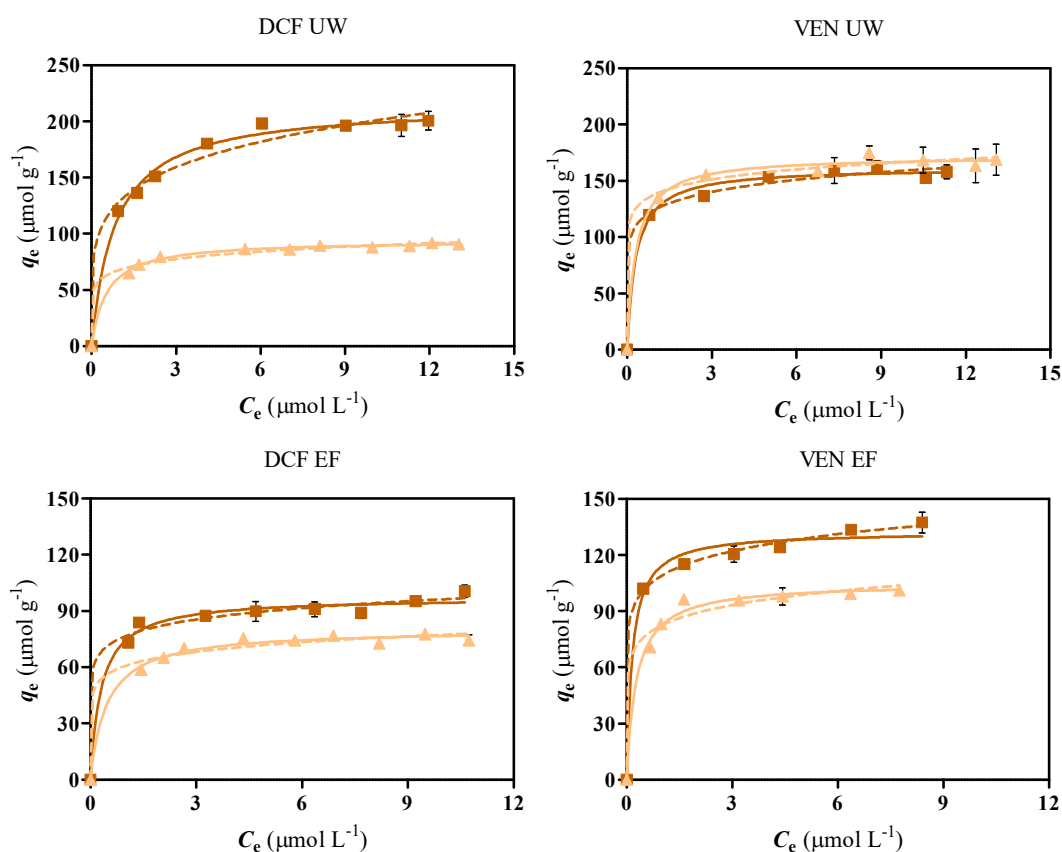
**Figure 4.** Equilibrium data for DCF and VEN in UW and EF using MAC-CP (■) and MAC-MW (▲) at 25 °C, together with modelling results: Langmuir (continuous lines, — and —) and Freundlich (dashed lines, --- and ---) isotherms. Note that *yy*-axis scale is different for UW and EF to allow a better visualization of results. Data points are the average of three independent experiments, with error bars representing standard deviations.

4
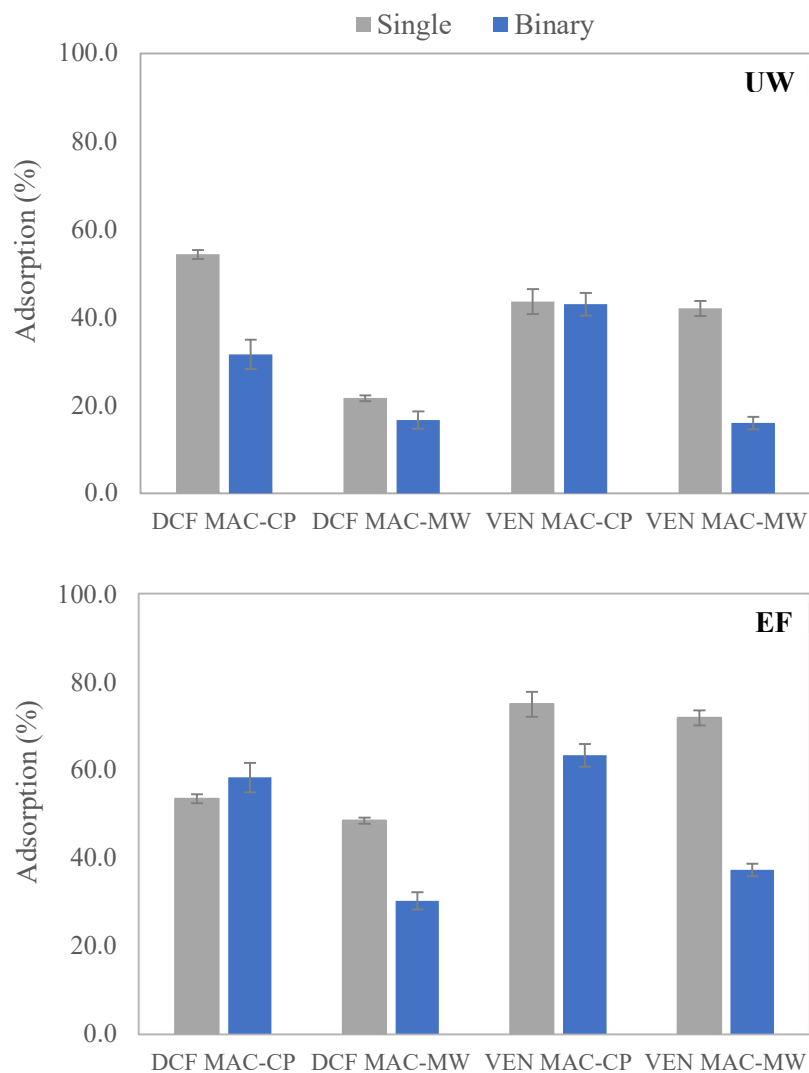
Figure 5. Adsorption percentage of DCF and VEN obtained for MAC-CP and MAC-MW in single and binary solutions (in UW and EF). Experimental conditions: C_{VEN}=14 μmol L^{-1}, C_{DCF}=14 μmol L^{-1} (single and binary solution), dose $_{MAC}$= 35 mg L^{-1} in UW and dose $_{MAC}$= 85 mg L^{-1} in EF. Data points are the average of three independent experiments, with error bars representing standard deviations.
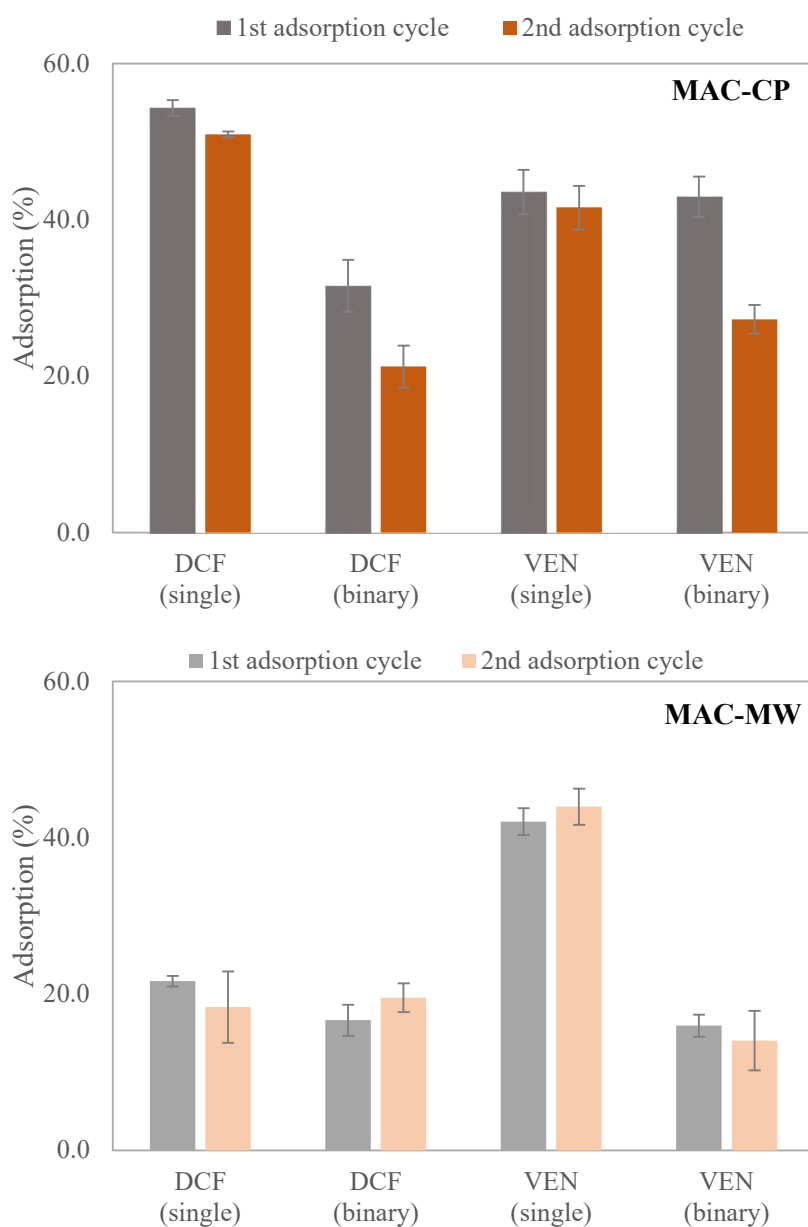
Figure 6. Adsorption percentage of DCF and VEN (single and binary solutions in UW) by virgin MAC-CP and MAC-MW (1st adsorption cycle) and after MW-assisted regeneration (2nd adsorption cycle). Experimental conditions: C_{VEN}=14 µmol L^{-1}, C_{DCF}=14 µmol L^{-1} (single and binary solution) and dose $_{MAC}$= 35 mg L^{-1}. Data points are the average of three independent experiments, with error bars representing standard deviations.

SUSTAINABLE AND RECOVERABLE IRON-CARBON MAGNETIC COMPOSITES FOR THE REMOVAL OF PHARMACEUTICALS FROM WASTEWATER

Luciana S. Rocha[1,*], Érika M.L. Sousa[1], Diogo Pereira[1], María V. Gil[2], Gonzalo Otero-Irurueta[3], María J. Hortigüela Gallo[3], Marta Otero[4], Valdemar I. Esteves[1], Vânia Calisto[1]

[1] *Department of Chemistry and CESAM, University of Aveiro, 3810-193 Aveiro, Portugal*

[2] *Instituto de Ciencia y Tecnología del Carbono, INCAR-CSIC, Francisco Pintado Fe 26, 33011 Oviedo, Spain*

[3] *TEMA-NRD, Mechanical Engineering Department, University of Aveiro, 3810-193 Aveiro, Portugal*

[4] *Department of Environment and Planning and CESAM, University of Aveiro, 3810-193 Aveiro, Portugal*

CONTENTS

Section S1. Analytic quantification of pharmaceuticals

The quantification of the pharmaceuticals in the aqueous solutions was carried out by MEKC, using a Beckman P/ACE MDQ (Fullerton, CA, USA) instrument, equipped with a UV-Vis detection system. A silica capillary was dynamically coated according to the procedure described in (Calisto et al., 2011). The electrophoretic separation was performed by direct polarity mode at 25 kV and 25 ºC, during 2.5 min for and DCF and during 5.0 min for VEN. All samples and standard solutions were spiked with the internal standard ethylvanillin (prepared previously by dissolution in acetonitrile/water (10/90 *v/v*)) at a final concentration of 3.34 mg L^{-1}. The detection was monitored at 200 nm. The separation buffer was composed by 15 mmol L^{-1} of sodium tetraborate and 50 mmol L^{-1} of SDS for DCF, and 15 mmol L^{-1} of sodium tetraborate and 15 mmol L^{-1} of SDS for VEN; the separation buffer was renewed every six runs. After each run, the capillary was washed with ultra-pure water (60 s) and then with the separation buffer (90 s), at 20 psi. The determination of the calibration curve was carried out for each pharmaceutical using seven standard solutions with concentrations ranging between 0.8 μmol L^{-1} and 17 μmol L^{-1} adjusted to pH 7.5±0.1. All the analyses were performed in quadruplicate.

Table S1. Proximate and ultimate analyses of primary sludge (PS) used as source for AC-CP and AA-MW production. Source: Jaria et al., 2019.
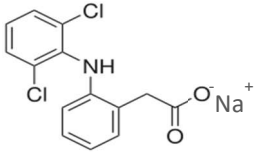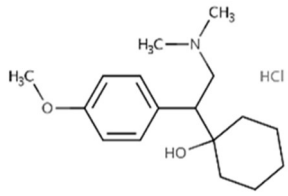
Proximate Analysis (db)[1]				Ultimate Analysis (dab)[2]					
Moisture (wt %)	Volatile Matter (wt %)	Fixed Carbon Content	Ash (wt %)	FC/VM	% C	% H	% N	% S	%O[3]
4.78	63.75	8.30	27.94	0.13	46.6	5.42	1.51	0.00	46.38

[1]Except for moisture, all values are presented in dry basis (*db*).

[2]Values are presented in dry and ash free basis (*dab*).

[3]Estimated by difference: %O=100-C-H-N-S.

Table S2. Physico-chemical properties of the pharmaceuticals under study.

Pharmaceutical		
Classe	Molecular structure	Properties
Non-steroidal anti-inflammatory drug		**Sodium diclofenac** M_w: 318.1 g mol^{-1} pk_a: 4.15
Antidepressant		**Venlafaxine hydrochloride** M_w: 313.9 g mol^{-1} pk_{a1}: 8.91; pk$_{a2}$: 14.42

1 https://go.drugbank.com/drugs/DB00586 (accessed in 22.01.2021)

2 https://go.drugbank.com/drugs/DB00285 (accessed in 22.01.2021)

Table S3. Binding energies (BE), their corresponding bond assignment and respective abundance (atomic %) of C 1s and O 1s peak, obtained from the respective fits (not showed).

C1s fit symmetric	C=C		sp3		C-O		C=O		O-C=O	
	BE	(%)	BE	(%)	BE	(%)	BE	(%)	BE	(%)
AC-CP	284.5	49.8	285.4	14.2	286.2	19.1	287.6	8,3	289.6	8.6
MAC-CP	284.6	55.3	285.4	9.7	286.1	21.9	287.8	6.0	289.3	7.1
AC-MW	284.5	60.6	285.4	8.9	286.2	14.0	287.8	10.9	289.7	5.6
MAC-MW	284.6	30.4	285.4	33.9	286.3	18.7	287.6	8.6	289.4	8.4

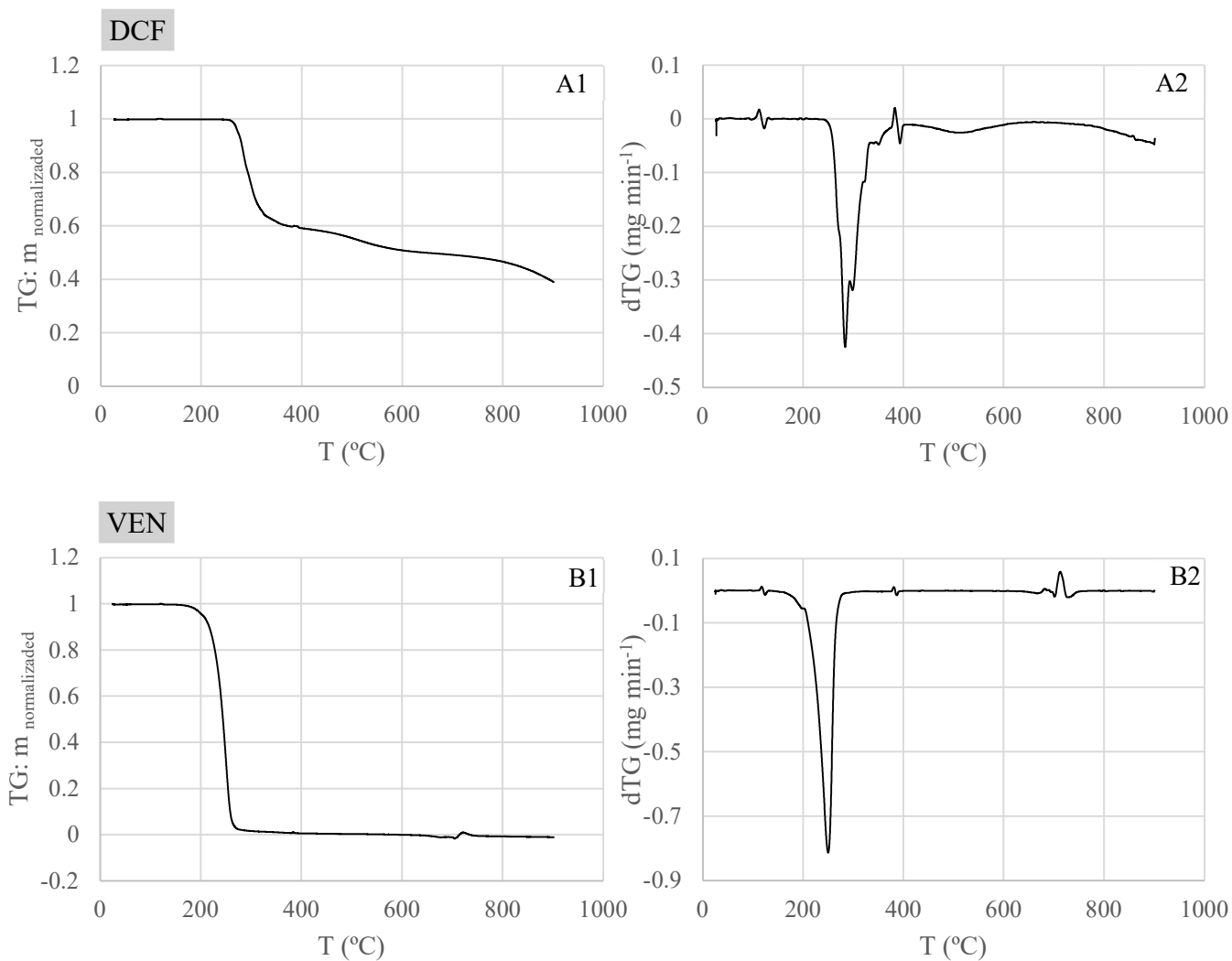| O1s fit	Fe–O		Fe–OH, C=O (aromatic)		Si–O, C–O, C=O (aliphatics, anhydrides)		O*–C=O, O=C–C–O*, C=O		H_2O	
	BE	(%)	BE	(%)	BE	(%)	BE	(%)	BE	(%)
AC-CP	-	-	531.0	22.4	532.8	41.1	534.0	30.4	535.5	6.1
MAC-CP	530.3	38.3	531.2	37.8	532.4	15.8	533.6	5.7	535.2	2.4
AC-MW	-	-	531.0	12.1	532.8	56.2	533.9	16.7	535.4	15.0
MAC-MW	530.5	32.1	531.5	32.2	532.4	22.0	533.5	12.5	535.0	1.2

Figure S1. Thermogravimetric (TG, m $_{normalized}$ corresponds to the mass normalized) and derivative thermogravimetric (dTG) profiles determined for DCF and VEN. The TGA analysis were performed under nitrogen atmosphere and using a heating rate of 10 °C min^{-1}.
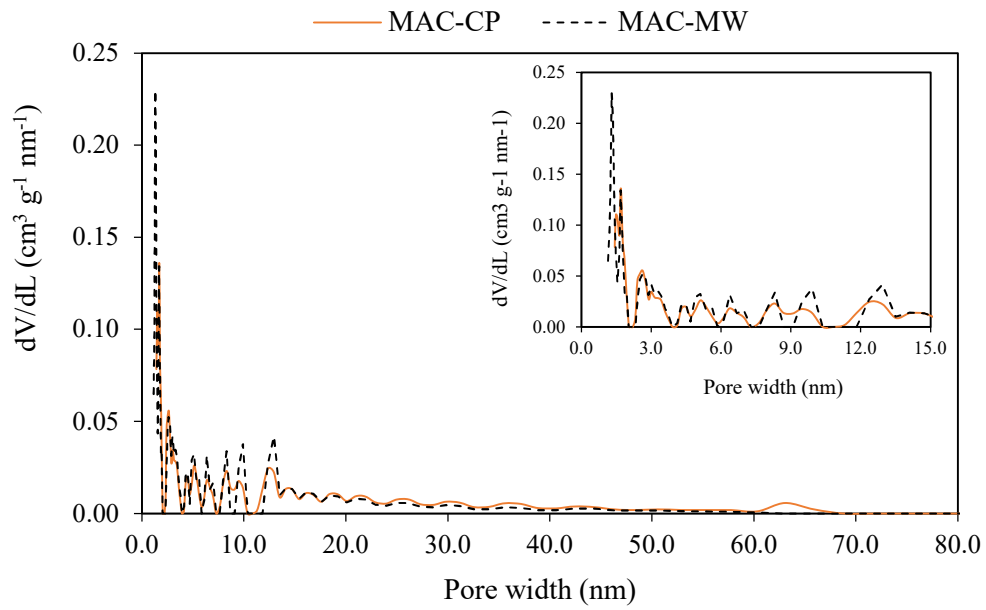
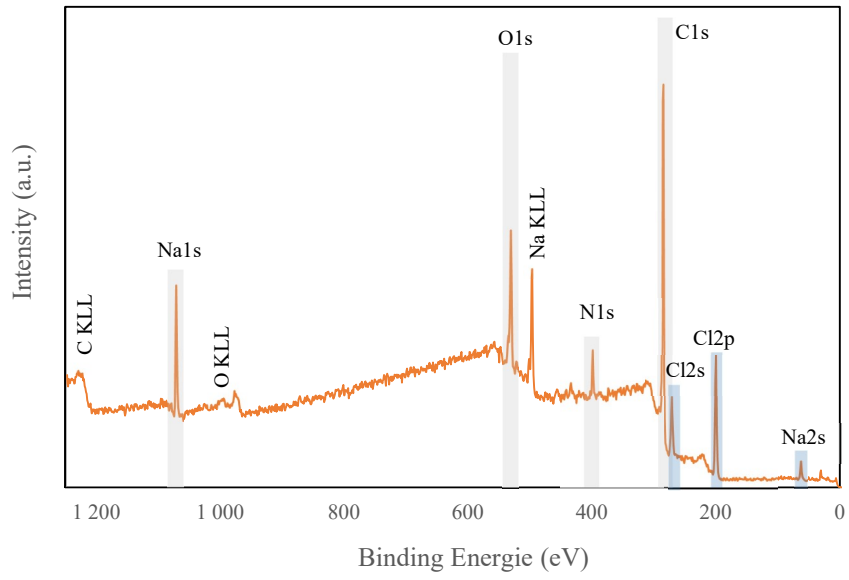**Figure S2.** Pore size distribution of MAC-CP and MAC-MW.
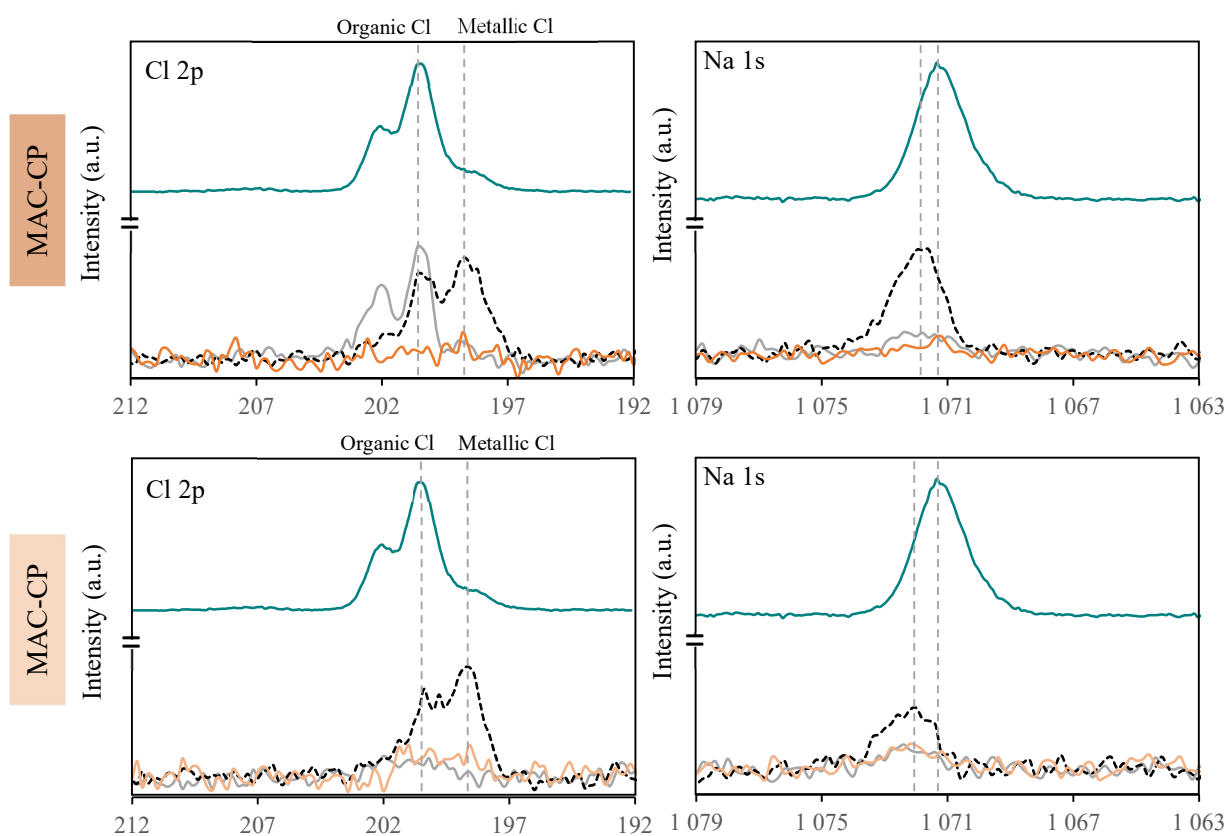
Figure S3. XPS spectrum of DCF.

Figure S4. XPS spectra of Cl 2p and Na 1s of DCF (——) and MAC, either MAC-CP or MAC-MW, at different stages: virgin (—— and ——), after the 1st adsorption cycle (——) and after MW-assisted regeneration (---).
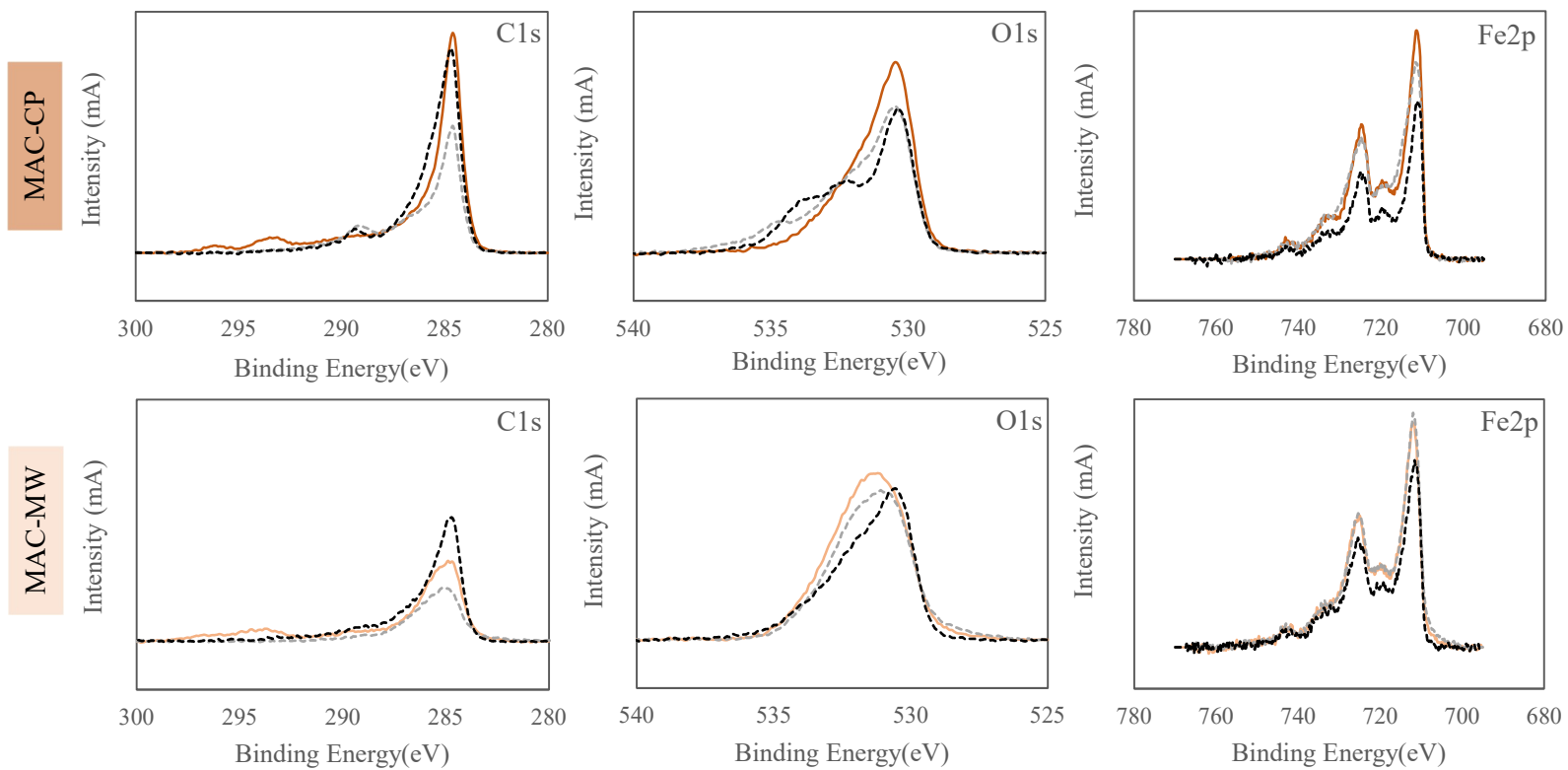
Figure S5. Comparison of the C1s, O1s and Fe2p core levels of XPS spectra obtained for MAC-CPand MAC-MW in several stages: virgin materials (── and

──), after the 1st DCF adsorption cycle (---) and after MW-assisted regeneration (---).